

~~CONFIDENTIAL~~

Copy  
RM L57E14

NACA RM L57E14

7777



10412  
JUL - 9 1957

0144813



TECH LIBRARY KAFB, NM

# RESEARCH MEMORANDUM

THE AERODYNAMIC CHARACTERISTICS OF A BODY IN THE  
TWO-DIMENSIONAL FLOW FIELD OF A  
CIRCULAR-ARC WING AT A MACH  
NUMBER OF 2.01

By John P. Gopcynski and Harry W. Carlson

Langley Aeronautical Laboratory  
Langley Field, Va.

~~This report contains information which is classified in the meaning of the espionage laws, Title 18, U.S.C., Secs. 793 and 794, the transmission or revelation of which in any~~

NATIONAL ADVISORY COMMITTEE  
FOR AERONAUTICS

WASHINGTON

July 2, 1957

~~CONFIDENTIAL~~

10412  
JUL - 9 1957



## NATIONAL ADVISORY COMMITTEE FOR AERONAUTICS

## RESEARCH MEMORANDUM

THE AERODYNAMIC CHARACTERISTICS OF A BODY IN THE  
TWO-DIMENSIONAL FLOW FIELD OF A  
CIRCULAR-ARC WING AT A MACH  
NUMBER OF 2.01

By John P. Gajcynski and Harry W. Carlson

## SUMMARY

A pressure-distribution investigation was conducted in the Langley 4- by 4-foot supersonic pressure tunnel to determine the aerodynamic characteristics of a body with a fineness ratio of 8 in the two-dimensional flow field of an  $8\frac{1}{3}$ -percent-thick circular-arc wing of rectangular plan form. Data were obtained for several wing-body positions at a Mach number of 2.01 and a Reynolds number of  $3.4 \times 10^6$  per foot.

Fairly good predictions of the trend and order of magnitude of the forces on the body due to the effect of the wing flow field were obtained from slender-body theory. Shock-expansion methods as well as linear theory were used to determine the wing-flow-field characteristics. Although the accuracy of the results of total drag and the normal-force loading was improved with the use of the more exact flow-field prediction, no appreciable improvement was noted in the results of total normal force and pitching moment.

No estimation was made of the total loads on the wing due to the effect of the body. The lack of sufficient experimental data and the unknown reflection characteristics of the wing shocks from the body surface precluded a rigorous analysis.

## INTRODUCTION

The prediction of the aerodynamic characteristics of wings and bodies in combination is difficult because of the complex nature of the interference effects which are involved. Two distinct problems are presented: First, the determination of the flow field in which the body or

wing surface is acting, and second, the determination of the characteristics of these surfaces in this field. In attempting to assess the validity of the use of existing theory in obtaining the characteristics of a body or wing in a nonuniform field, it would be advantageous, at first, to work with relatively simple flow fields. In this way, a much more fundamental understanding of the wing-body problem may be gained.

With this purpose in mind, an investigation is being conducted in the Langley 4- by 4-foot supersonic pressure tunnel to determine the characteristics of bodies and wings in flow fields with varying degrees of complexity. The first phase of this investigation was reported in reference 1, wherein the changes in the aerodynamic characteristics of a body were determined as the position of the body was varied with respect to a flat plate aligned with the airstream. It was found that the prediction of the chord-force increments (due to interference effects) and the prediction of the variation and order of magnitude of the normal-force increments was very good. These results were obtained by the application of slender-body theory as outlined by Moskowitz in reference 2.

The present report is concerned with the characteristics of a body in the two-dimensional flow field of a circular-arc wing of rectangular plan form. The effect of the body field on the wing is also considered, although the analysis in this case is not extensive. Pressure measurements on the body and the wing have been obtained for a range of body positions with respect to the wing, both in a chordwise and a vertical (with respect to the chord plane) direction, and for wing angles of attack of  $0^\circ$  and  $5^\circ$ . Tests were made at a Mach number of 2.01 and a Reynolds number of  $3.4 \times 10^6$  per foot. The data are compared with theoretical results.

#### SYMBOLS

$\rho$	mass density of air
$V$	airspeed
$a$	speed of sound in air
$M$	Mach number, $V/a$
$q$	dynamic pressure, $\frac{1}{2}\rho V^2$
$p$	free-stream static pressure

- $P_1$  local static pressure
- $C_p$  pressure coefficient,  $\frac{P_1 - p}{q}$
- $\Delta C_p$  increment in pressure coefficient due to the effect of an interference field
- $\beta = \sqrt{M^2 - 1}$
- $R$  local radius of body
- $L$  length of body
- $c$  wing chord length
- $\theta$  body polar angle, deg (see fig. 1)
- $x$  distance from apex of body measured along axis of symmetry
- $\alpha_w$  angle of attack of wing, deg
- $X$  chordwise position of body nose with respect to wing midpoint (positive when measured upstream)
- $Z$  vertical position of body nose with respect to wing chord plane
- $S$  body cross-sectional area
- $m(\xi)$  distribution function
- $\phi$  potential
- $r$  distance normal to body axis
- $\xi$  integration variable
- $\bar{u}, \bar{v}, \bar{w}$  perturbation velocity components of disturbance field
- $c_n$  body-section normal-force coefficient,  $\frac{\text{Body section normal force}}{2qR}$
- $C_N$  body normal-force coefficient (positive towards wing),  $\frac{\text{Body normal force}}{qS_{\max}}$

- $C_m$  body pitching-moment coefficient (about apex of body),  

$$\frac{\text{Body pitching moment}}{qS_{\max}L}$$
- $\Delta C_c$  interference increment in body pressure chord-force coefficient,  $\frac{\text{Body chord-force increment}}{qS_{\max}}$
- $\Delta C_{N,w}$  interference increment in wing normal-force coefficient (based on unit span),  $\frac{\text{Wing normal-force increment}}{qc}$
- $\Delta C_{c,w}$  interference increment in wing chord-force coefficient (based on unit span),  $\frac{\text{Wing chord-force coefficient}}{qc}$

## Subscripts:

max maximum

b body base

## DESCRIPTION OF MODELS AND TESTS

The test setup is shown in figure 1. An  $8\frac{1}{3}$ -percent-thick circular-arc wing of rectangular plan form was mounted from the tunnel side wall on two sweptback struts. Three rows of pressure orifices (23 orifices per row) were provided on the surface of the wing nearest the body. Longitudinal motion (chordwise) between the wing and the body was accomplished by movement of the wing along the tunnel side wall.

The fuselage model was a blunt-based parabolic body of revolution with a length equal to that of the wing chord and with a fineness ratio of 8. The body was equipped with two rows (located  $180^\circ$  apart) of static-pressure orifices. Each row contained 24 orifices. Provision was made in the model sting for rolling the body about its own axis so that complete pressure coverage could be obtained. Lateral motion between the body and the wing (Z direction, fig. 1) was obtained by translation of the body and sting.

Pressure measurements on the body and the wing were obtained for the six chordwise and four vertical body-wing positions shown on the test grid in figure 1. Tests were made for a body angle of attack of  $0^\circ$

and wing angles of attack of  $0^\circ$  and  $5^\circ$ . The test Mach number was 2.01 and the Reynolds number,  $3.4 \times 10^6$  per foot. Throughout the test, transition strips (No. 60 carborundum grains) were installed on both the body and the wing.

Tunnel stagnation conditions were as follows: temperature,  $110^\circ$  F; dewpoint, approximately  $-35^\circ$  F; and pressure, 14 pounds per square inch absolute.

## RESULTS AND DISCUSSION

### Presentation of Data

The basic data obtained on the body and wing are presented in figures 2 and 3, respectively. The pressure-coefficient variation on the body is presented as a function of the body station and radial angle for each of the body-wing positions investigated. The pressure-coefficient variation on the wing is presented as a function of the wing station for the orifice rows indicated in figure 1. In each case the data for a wing angle of attack of  $0^\circ$  are presented in the upper portion of the figure and those for an angle of  $5^\circ$ , in the lower portion.

In order to aid in the interpretation of these data and to gain a fundamental understanding of the actual flow phenomena which are taking place, the pressure distribution on the body meridian closest to the wing ( $\theta = 180^\circ$ ) and the distribution on the wing directly opposite the body (Row 1) are shown in figure 4 for the six chordwise positions used during the test. The vertical distance between the wing-chord plane and the body center line in this case is 2.5 inches. The solid line on the pressure-distribution plots represents the experimental interference-free data. For reasons which are discussed subsequently, Mach lines are used to establish the region of influence of the body, and the leading-edge shock wave (determined from shock-expansion theory) is used to indicate the influence of the wing. Although the multiple shock reflections which are shown between the wing and the body in figure 4 are only qualitative in nature, they do serve to identify the origin of the abrupt changes in pressure which exist on the wing and the body.

It is of interest to note that at position  $X = 8$  the reflection of the wing leading-edge shock from the body back on the wing produces a pressure increase of the same order of magnitude as the effect of the body shock on the wing. Also, for chord position 3,  $X = 4$ , it is apparent from the magnitude of the pressure increase on the wing that the reflected wing shock and the body shock have coalesced on the wing surface. The pressure increase on the rearward portion of the body at chord position 6,  $X = -8$ , is due to the reflection of the wing leading-edge shock from the tunnel side wall. The presence of this reflected

shock must, of necessity, invalidate the data at small values of  $Z$  for chord positions 5 and 6, that is,  $X = -4$  and  $-8$ , respectively.

### Analysis

One of the initial problems which was encountered in the analysis of the present wing-body problem was the accurate definition of the flow field in which the body was acting. This problem becomes more acute as the body is moved away from the wing, as may be seen from an examination of figure 5. In this figure the flow-field boundaries of an  $8\frac{1}{3}$ -percent-thick wing are shown. The experimental points which identify the leading- and trailing-edge shocks were determined from the body pressure distributions and, for the case of the leading-edge shock, are in good agreement with the results obtained from shock-expansion methods. In contrast, it may be noted that the wing flow field defined by Mach lines (linear theory) is not an adequate representation of actual conditions. In order to illustrate the effect of these flow-field differences on the prediction of body forces, comparisons between experiment and theory are made for each method of flow-field definition.

The predictions of the forces on the body in the wing flow field were determined from slender-body theory. This development is presented in the appendix and follows that given in reference 2. It is shown that the lift of a body in a nonuniform flow field is a function of the buoyant and upwash effects of that field.

In the determination of the buoyant forces, contour maps of the wing pressure field were used. The body was superimposed in this field (with the assumption that the field was not disturbed in any manner) and the incremental pressures at the body surface were used to compute the interference increments in normal force, drag (chord force), and pitching moment. The graphical method was used in anticipation of increased accuracy in the normal-force results, particularly with respect to the distribution of this force. Actually, the results obtained from equation (9) for the total buoyant forces on the body were in excellent agreement with those obtained graphically.

For the estimation of drag, the aforementioned approach is similar to that used in reference 3, except that in the present case the surface pressures on the body were used rather than those which exist in the location of the body center line. It was found in reference 1 that the differences involved were negligible, and inasmuch as surface pressures had to be determined for lift calculations, they were also used for the drag results.

The lift, or normal force, due to the upwash effects of the field is shown in equation (7) to be dependent only on the upwash and cross-sectional area at the base of the body. The appropriate values of upwash were obtained from the contour plots of the wing flow field. The distribution of this normal force was obtained from application of equation (9) with the use of a center-line distribution of upwash.

### Body Characteristics

The changes in the aerodynamic characteristics of the body due to the effect of the wing flow field are presented in figure 6 as functions of the position of the body with respect to the wing. Inasmuch as the experimental results in this figure are compared with an analysis based upon the linearized wing flow field, the wing-body position is defined by the parameter  $X + \beta Z$ . Thus, movement of the body along any Mach line emanating from the wing will result in a constant value of  $X + \beta Z$ . As the body is moved into the wing flow field (from wing leading edge to trailing edge) it is first subject to a negative, or favorable, chord-force increment, a negative normal force tending to move the body away from the wing, and a corresponding positive moment about the nose. Further movement of the body into the wing field results in a reversal of each of these trends, the maximum values in this case occurring when the body is completely immersed in the field ( $X + \beta Z \cong 6$ ). As the body is moved out of the field it is again subject to a reversal in the signs of the forces and moment. In general, the results for a wing angle of attack of  $5^\circ$  are similar to those for  $0^\circ$ .

The experimental results in this figure are compared with the analysis based upon the linearized wing flow field. The dashed line in each case represents that portion of the estimated overall force or moment which is due to the buoyant effect of the field. The solid line represents the total estimated normal force and pitching moment and is obtained by the addition of the increment due to the upwash of the field to the buoyant value.

In general, the prediction of the trend and order of magnitude of the forces and moments is very good. It should be noted, however, that the estimation of the actual values at any particular wing-body position may be subject to large error.

The effect of the discrepancies which exist between the actual and the linearized flow fields is not readily apparent from the data except for the variation in drag. In this case, there is a noticeable shift between the experimental and theoretical curves. In order to determine the effect of the flow-field differences on the normal-force variation, the distribution of loading over the body must be examined. For this purpose, the increments in pressure coefficients ( $\theta = 0^\circ$  and  $180^\circ$ )

due to the interference effects of the wing and the normal-force distributions along the body are presented in figure 7 for four representative positions of the body in the wing flow field. The positions were chosen to illustrate the effects of leading- and trailing-edge shock impingement on the body, complete immersion of the body in the flow field, and the effect of multiple reflections between the wing and the body. The dashed line again represents the magnitude of the buoyant effects of the field and the solid line, the addition of the upwash effects to the buoyancy results. It should be noted that an impulsive force (see appendix) must be added to the results at the intersection points of the wing leading- and trailing-edge shocks with the body center line. The line of action of this force is indicated by the arrow on the normal-force loading distributions of figure 7.

From an examination of figure 7 it may be seen that the use of a linearized field, in this case, resulted in a poor estimation of the load distribution over the body. The effect of the difference in the actual and predicted flow fields is readily apparent in the point of origin of the wing disturbance on the body. It should be noted, however, that integration of the theoretical load distributions may give results which are consistent with experimental data. This is particularly true of the buoyancy results which form the larger part of the normal force to which the body is subject.

The results which may be obtained with the use of a more accurate representation of the flow field are shown in figure 8. Data are presented for the four representative wing-body positions discussed previously, and comparisons are made with an analysis based on shock-expansion methods of flow-field definition. The estimation of body pressures and normal-force loadings is fairly good except in the region of the impulsive loading. Further improvements may be possible if additional refinements to the flow field are made. The pressure increments due to upwash were determined from conditions along the body center line and thus do not accurately define the conditions at the body surface. Use of surface upwash values might possibly have improved the agreement between results. In addition, more accurate values of the loading might have been obtained in some cases by a consideration of the multiple reflections of shock waves between the body and wing. These applications are tedious, however, and do not appear to be warranted.

The estimated total force and moment characteristics of the body, based on shock-expansion flow-field calculations, are compared with the experimental results in figure 9. Because of the lack of data it is difficult to determine whether the prediction of actual values of normal force and pitching moment has been improved with the use of the more exact flow-field calculations. The estimation of the trends of these curves, however, does appear to be more accurate. This is particularly true at the larger values of the wing-body separation distance. The

prediction of the drag characteristics shows considerable improvement in the agreement with the experimental results.

With regard to the normal-force values, it should be noted that small opposing differences in the predictions of body pressures may result in substantial variations in the integrated values of body normal force. Thus, even though the estimation of body pressures may be fairly representative of the experimental results, no improvement in the total-force values may be obtained.

### Wing Characteristics

The main emphasis of this report has been placed on the determination of the change in body characteristics due to the action of a non-uniform flow field and, in this respect, the wing has served only as a generator of this field. It is also of interest, however, to examine the effect of the body on the wing. The variations in wing normal force and chord force are presented in figures 10(a) and 10(b), respectively, as functions of wing-body position. Because the amount of experimental data obtained on the wing was limited, the results should be regarded as qualitative in nature. In addition, data were obtained only on the wing surface next to the body and, therefore, the results for those positions where the wing is completely immersed in the body field are not complete.

For body positions near the wing (small values of  $z$ ), the interference increments in wing chord force (fig. 10(b)) are predominately unfavorable. Movement of the body away from the wing, however, tends to reverse this condition. The normal-force results (fig. 10(a)) indicate conditions of favorable lift interference except for forward body positions at small values of the wing-body separation distance. The results at these forward body positions are not complete, however, inasmuch as the effect of the body flow field on both sides of the wing is not known.

The most advantageous body-wing position for favorable interference must be determined from a consideration of both wing and body results. For example, for rearward body positions at small values of  $z$ , the wing and body drag increments are negative and the normal-force values are positive and negative, respectively. Although this is a region of favorable drag interference, it may not be a good region for favorable lift-drag ratios because of the negative normal-force increments on the body.

The prediction of the interference effects on the wing is a complex problem for the present configuration. In order to analyze this situation, wing-interference pressure increments are presented in figure 11 for four representative positions. The theoretical curve represents the pressures which would exist on a flat plate in the wing-chord plane and, as such, is a first approximation to the wing surface pressures.

It is readily apparent that sizable corrections to the flow field are necessary for dependable force predictions. It is equally apparent, however, that some of these corrections are not simply defined.

Considerable improvement in the pressure distributions may be possible with a more accurate definition of the body flow field and from a determination of conditions at the wing surface rather than at the chord plane. Several simplifying assumptions must be made, however, since a rigorous analysis by three-dimensional characteristics does not appear to be warranted. It should also be noted that the reflection characteristics of the wing leading-edge shock from the body are unknown. Inasmuch as the pressure rise from this source may be quite large, the problem of multiple shock reflection cannot be ignored. In view of these complexities, no attempt was made to predict the interference increments in total wing forces.

#### CONCLUDING REMARKS

The changes in the aerodynamic characteristics of a blunt-based parabolic body of revolution with a fineness ratio of 8 have been determined in the two-dimensional flow field of an  $8\frac{1}{3}$ -percent-thick circular-arc wing of rectangular plan form. Data were obtained at a Mach number of 2.01, a Reynolds number of  $3.4 \times 10^6$  per foot, and at wing angles of attack of  $0^\circ$  and  $5^\circ$ . The results were compared with theoretical values obtained from the application of slender-body theory. Shock expansion, as well as linear theory, was used to define the wing flow field.

Fairly good predictions of the trend and order of magnitude of the forces on the body due to the presence of the wing flow field were possible with the application of slender-body theory. The use of shock-expansion methods in defining the wing flow field did not appreciably improve the accuracy of the estimations of total body normal force and pitching moment over those given by the use of linearized methods. The accuracy of the predictions of normal-force loading and total drag, however, was dependent upon the method of flow-field definition, the results obtained from shock-expansion theory being in better agreement with the experimental data than those obtained from linear theory.

No estimation was made of the total loads on the wing due to the effect of the body. The lack of sufficient experimental data and the unknown reflection characteristics of the wing shocks from the body surface precluded a rigorous analysis. The body effect on the wing

~~CONFIDENTIAL~~

must be considered in any estimation of wing-body loads, however, inasmuch as positions for favorable body effects may not result in favorable overall lift-drag ratios.

Langley Aeronautical Laboratory,  
National Advisory Committee for Aeronautics,  
Langley Field, Va., April 24, 1957.

CONFIDENTIAL  
~~CONFIDENTIAL~~

## APPENDIX

## PREDICTION OF FORCES ON A BODY IN A NONUNIFORM FLOW FIELD

If a slender body of revolution at zero angle of attack in a uniform supersonic stream of velocity  $V$  is subject to a small disturbance field ( $\bar{u}$ ,  $\bar{v}$ ,  $\bar{w}$ ), the pressure which contributes to the lift of the body is shown in reference 2 to be given by the expression

$$C_p = -\frac{2\phi_x}{V} - \frac{2\bar{u}}{V} \quad (1)$$

The potential  $\phi$  is that part of the total velocity potential (due to the disturbance field) which contributes to lift and is dependent only on the upwash  $\bar{w}$ . Thus, it may be seen that the lift of a body in a disturbance field is a function of the upwash and buoyant effects of that field.

The potential may be written as

$$\phi = -\frac{\cos \theta}{r} \int_0^{x-\beta r} \frac{m(\xi)(x-\xi)d\xi}{\sqrt{(x-\xi)^2 - \beta^2 r^2}} \quad (2)$$

where the distribution function  $m(\xi)$ , when related to the local cross-flow ( $r \rightarrow 0$ ), is equal to the expression

$$m(\xi) = \frac{d}{dx} (R^2 \bar{w}) \quad (3)$$

From equations (1), (2), and (3), by using the approximation that the body radius approaches 0, the lifting pressure due to the upwash field may be obtained as

$$C_{p, \text{upwash}} = \frac{2 \cos \theta}{VR} \frac{d}{dx} (R^2 \bar{w}) \quad (4)$$

The lifting pressure due to the buoyant effect of the disturbance field is shown in reference 2 to be given by the following expression

$$C_{p, \text{buoyancy}} = \frac{2}{V} R \cos \theta \frac{d\bar{w}}{dx} \quad (5)$$

It should be noted that this term results from an expansion of  $\bar{u}$  in a Taylor's series and a consideration of the irrotationality of the flow.

The total normal-force coefficient on the body may then be expressed as

$$C_N = \frac{2}{S_{\max}} \int_0^L \left\{ S(x) \frac{d}{dx} \left( \frac{\bar{w}}{V} \right) + \frac{d}{dx} \left[ S(x) \frac{\bar{w}}{V} \right] \right\} dx \quad (6)$$

where the first term under the integral sign represents the contribution of the buoyant effect of the field to the lift, and the second term represents the upwash portion. Equation (6) may thus be expressed as

$$C_N = \frac{2}{S_{\max}} \int_0^L \left[ S(x) \frac{d}{dx} \left( \frac{\bar{w}}{V} \right) \right] dx + \frac{2S_b \bar{w}_b}{S_{\max} V} \quad (7)$$

In the derivation of this equation it was assumed that  $\bar{u}$ ,  $\bar{w}$ , and their derivatives were continuous. If this is not the case, some care must be used in evaluating the integrals of equation (6). If a discontinuity in  $\bar{w}$  is assumed at  $x = x_1$ , equation (6) becomes

$$\begin{aligned} C_N = & \frac{2}{S_{\max}} \int_0^{x_1-\delta} S(x) \frac{d}{dx} \left( \frac{\bar{w}}{V} \right) dx + \frac{2}{S_{\max}} \int_{x_1-\delta}^{x_1+\delta} S(x) \frac{d}{dx} \left( \frac{\bar{w}}{V} \right) dx + \\ & \frac{2}{S_{\max}} \int_{x_1+\delta}^L S(x) \frac{d}{dx} \left( \frac{\bar{w}}{V} \right) dx + \frac{2}{S_{\max}} \int_0^{x_1-\delta} \frac{d}{dx} \left[ S(x) \frac{\bar{w}}{V} \right] dx + \\ & \frac{2}{S_{\max}} \int_{x_1-\delta}^{x_1+\delta} \frac{d}{dx} \left[ S(x) \frac{\bar{w}}{V} \right] dx + \frac{2}{S_{\max}} \int_{x_1+\delta}^L \frac{d}{dx} \left[ S(x) \frac{\bar{w}}{V} \right] dx \quad (8) \end{aligned}$$

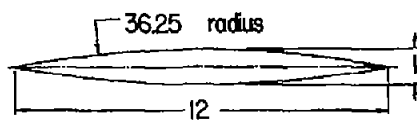
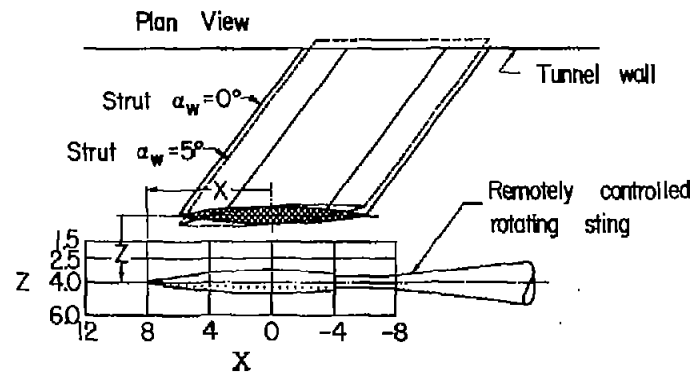
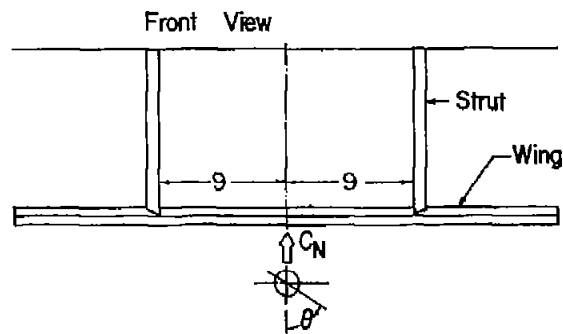
(where  $\delta$  is a small increment in  $x$ ) and on simplifying,

$$C_N = \frac{2}{S_{\max}} \left\{ \int_0^{x_1 - \delta} S(x) \frac{d}{dx} \left( \frac{\bar{w}}{V} \right) dx + \frac{S(x_1)}{V} \left[ \bar{w}(x_1 + \delta) - \bar{w}(x_1 - \delta) \right] + \int_{x_1 + \delta}^L S(x) \frac{d}{dx} \left( \frac{\bar{w}}{V} \right) dx \right\} + \frac{2}{S_{\max}} \left\{ \int_0^{x_1 - \delta} \frac{d}{dx} \left[ S(x) \frac{\bar{w}}{V} \right] dx + \frac{S(x_1)}{V} \left[ \bar{w}(x_1 + \delta) - \bar{w}(x_1 - \delta) \right] + \int_{x_1 + \delta}^L \frac{d}{dx} \left[ S(x) \frac{\bar{w}}{V} \right] dx \right\} \quad (9)$$

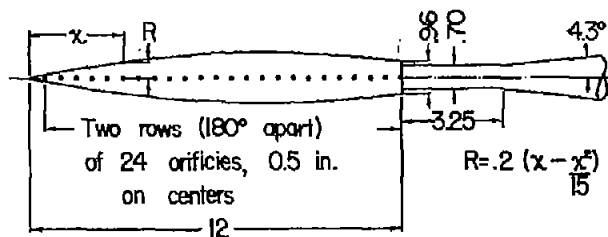
The terms in the first set of braces represent the buoyant contribution, and those in the second set, the upwash contribution. It should be noted that each contribution contains an impulsive force (represented by the term  $\frac{S(x_1)}{V} \left[ \bar{w}(x_1 + \delta) - \bar{w}(x_1 - \delta) \right]$ ) located at the point of flow discontinuity. It should also be noted that those terms which represent the upwash contribution will integrate to the value given in equation (7), that is,  $\frac{2S_b \bar{w}_b}{S_{\max} V}$ . Therefore, that portion of the body normal force due to the upwash of the disturbance field is dependent only upon the upwash at the base and the base area even though a discontinuity exists in the field.

## REFERENCES

1. Gapcynski, John P., and Carlson, Harry W.: A Pressure-Distribution Investigation of the Aerodynamic Characteristics of a Body of Revolution in the Vicinity of a Reflection Plane at Mach Numbers of 1.41 and 2.01. NACA RM L54J29, 1955.
2. Moskowitz, Barry: Approximate Theory for Calculation of Lift of Bodies, Afterbodies, and Combinations of Bodies. NACA TN 2669, 1952.
3. Friedman, Morris D., and Cohen, Doris: Arrangement of Fusiform Bodies To Reduce the Wave Drag at Supersonic Speeds. NACA Rep. 1236, 1955. (Supersedes NACA RM A51I20 by Friedman and TN 3345 by Friedman and Cohen.)



Wing Section  
8 1/2% thick circular arc



Body

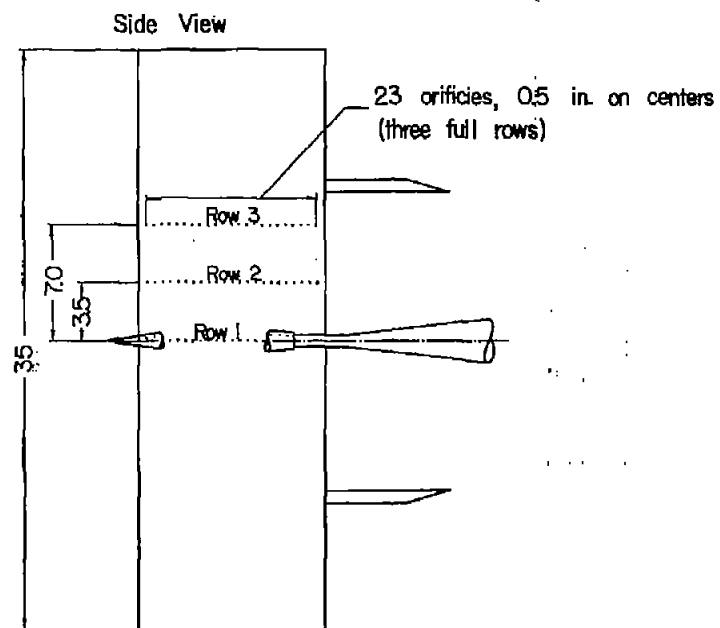
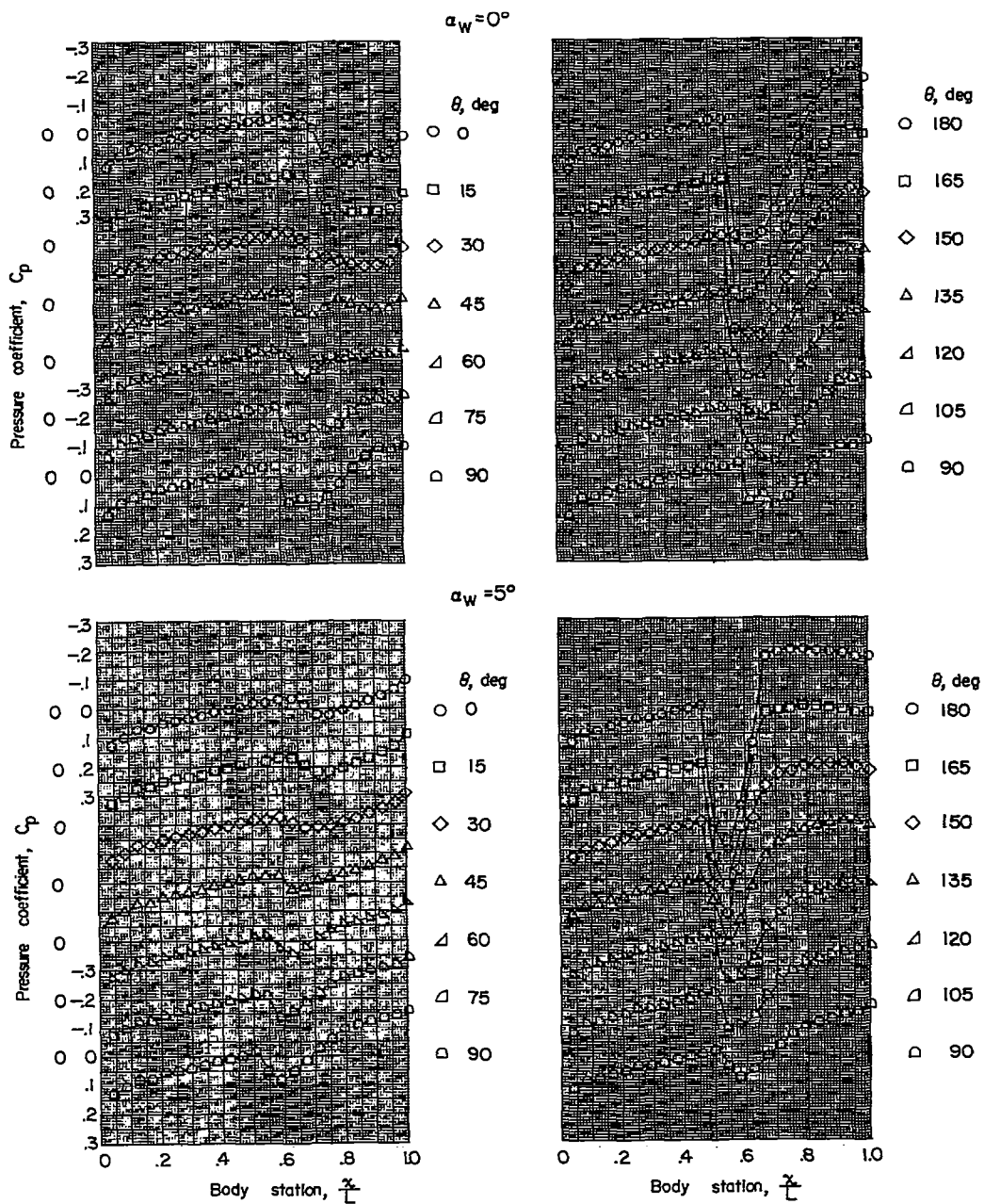
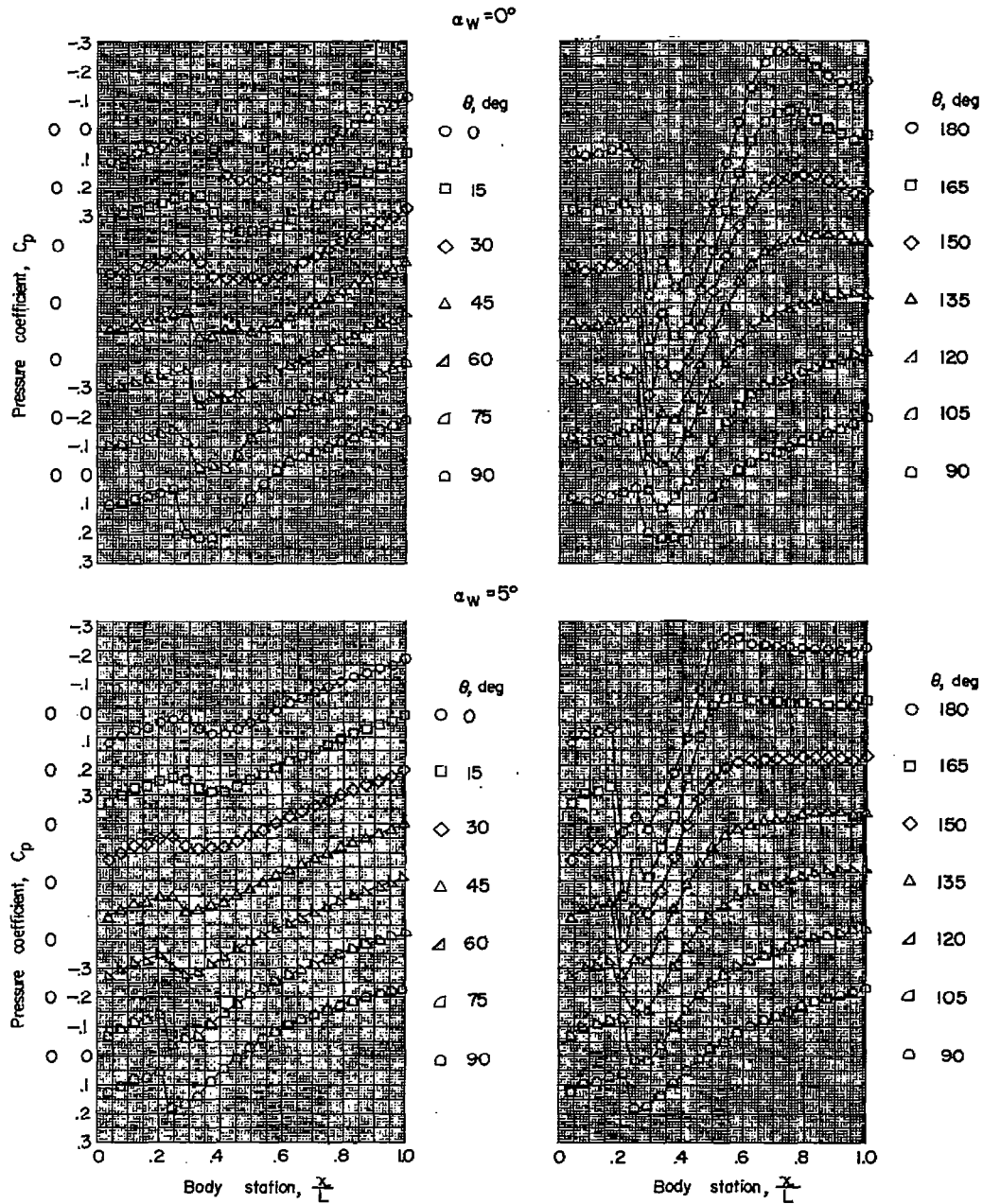


Figure 1.- Schematic layout of models and test setup. (All linear dimensions are in inches.)



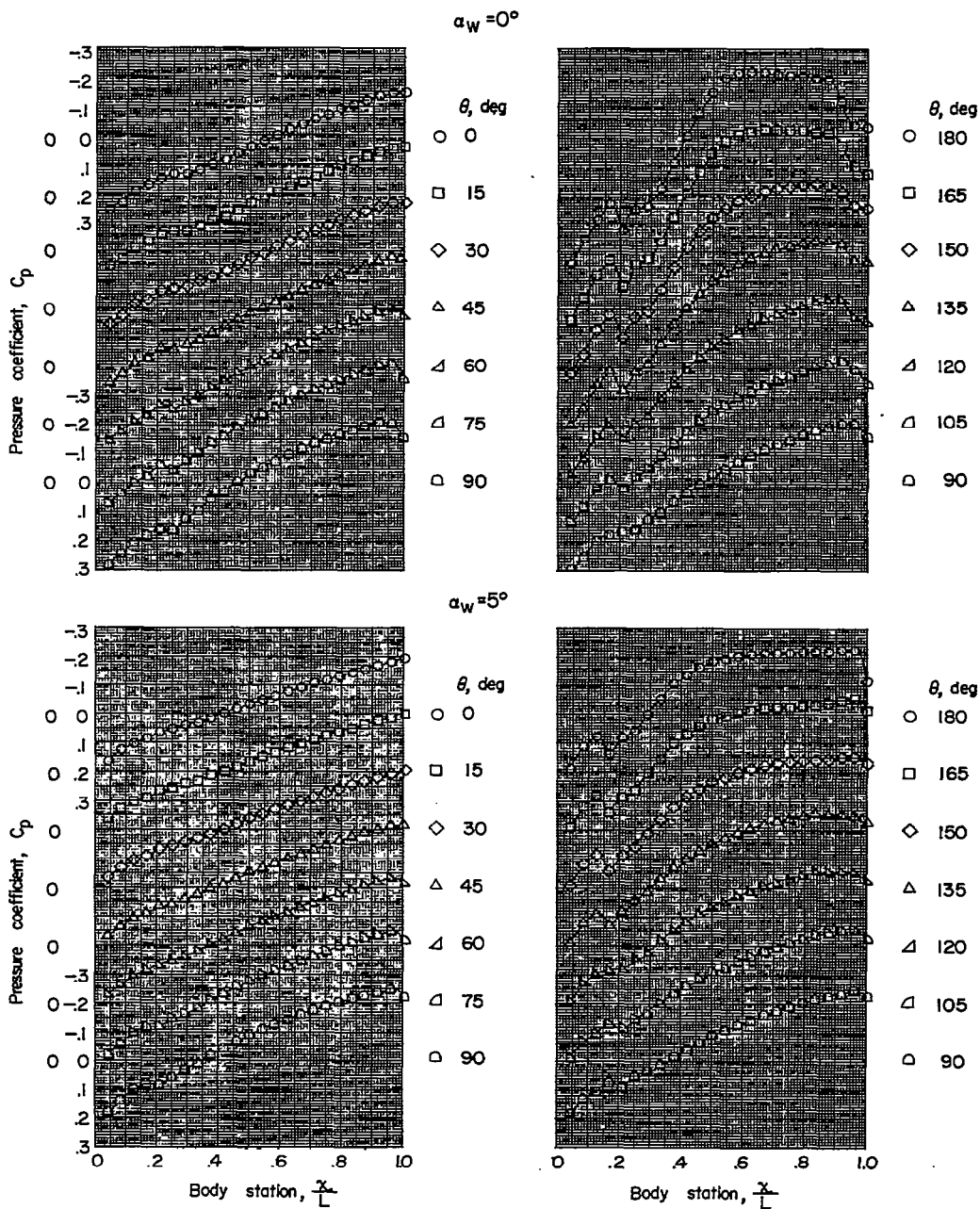
(a)  $X = 12; Z = 1.5$ .

Figure 2.- Pressure-coefficient variation on the body for the various wing-body positions investigated.



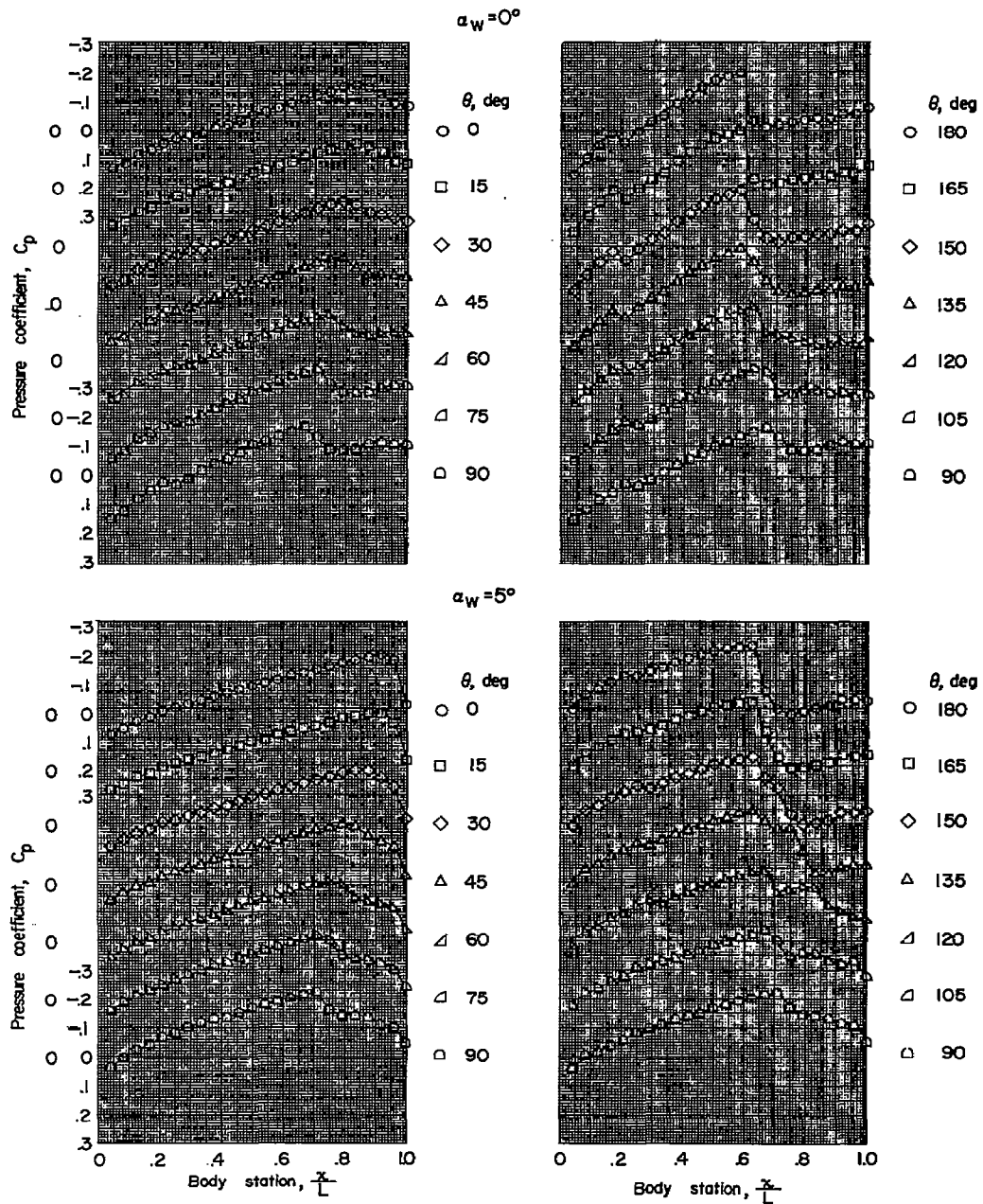
(b)  $X = 8$ ;  $Z = 1.5$ .

Figure 2.- Continued.



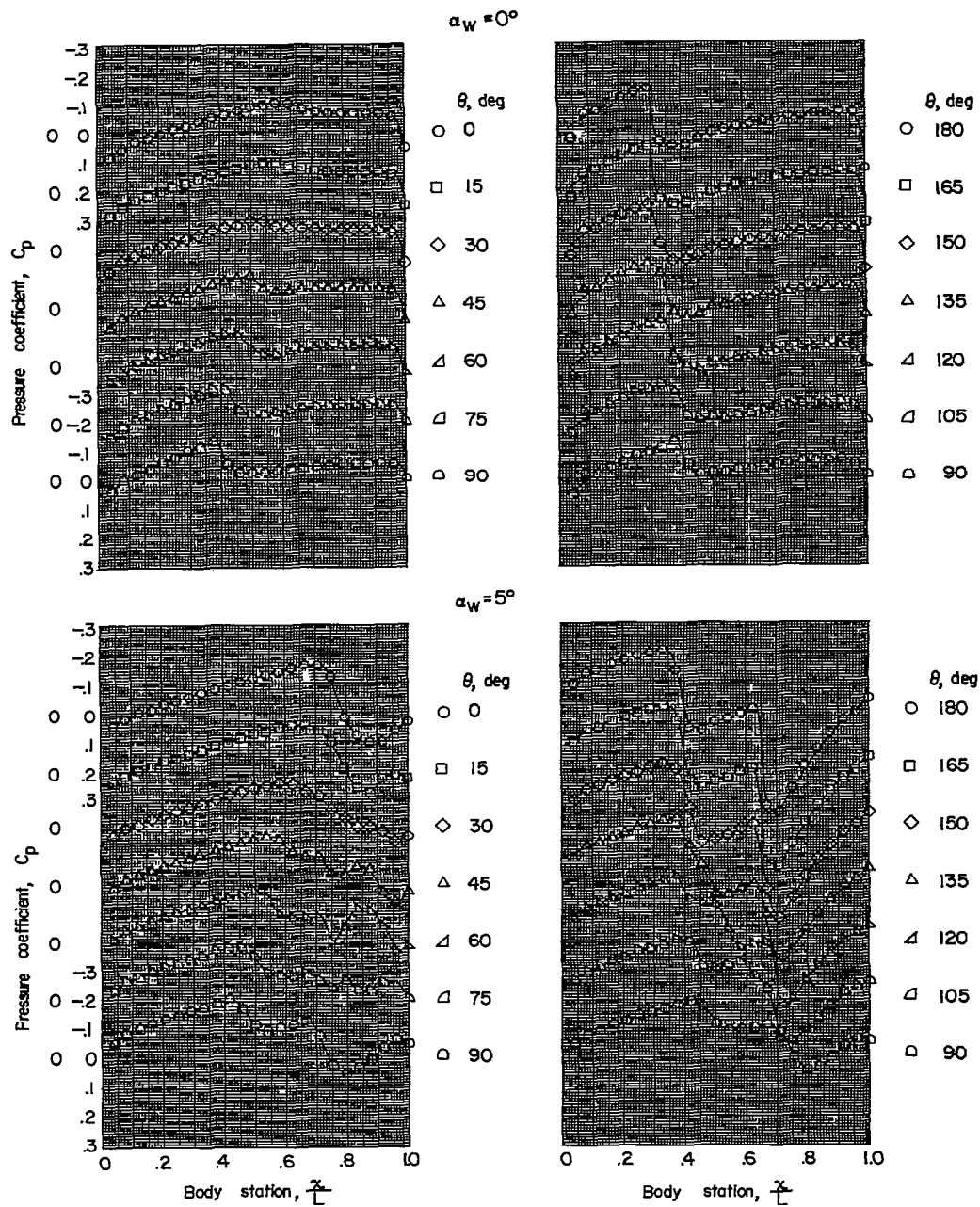
(c)  $X = 4$ ;  $Z = 1.5$ .

Figure 2.- Continued.



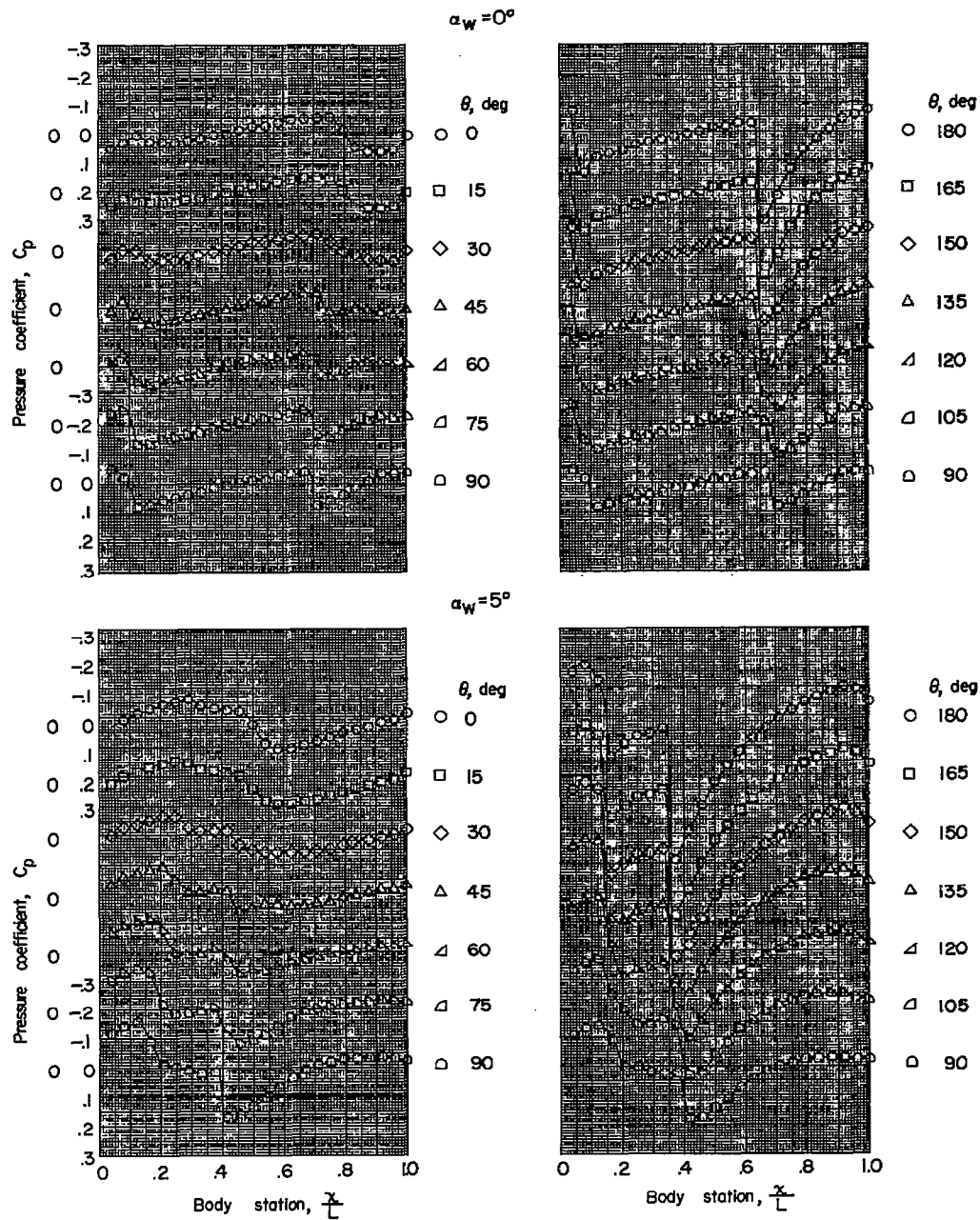
(d)  $X = 0; Z = 1.5$ .

Figure 2.- Continued.



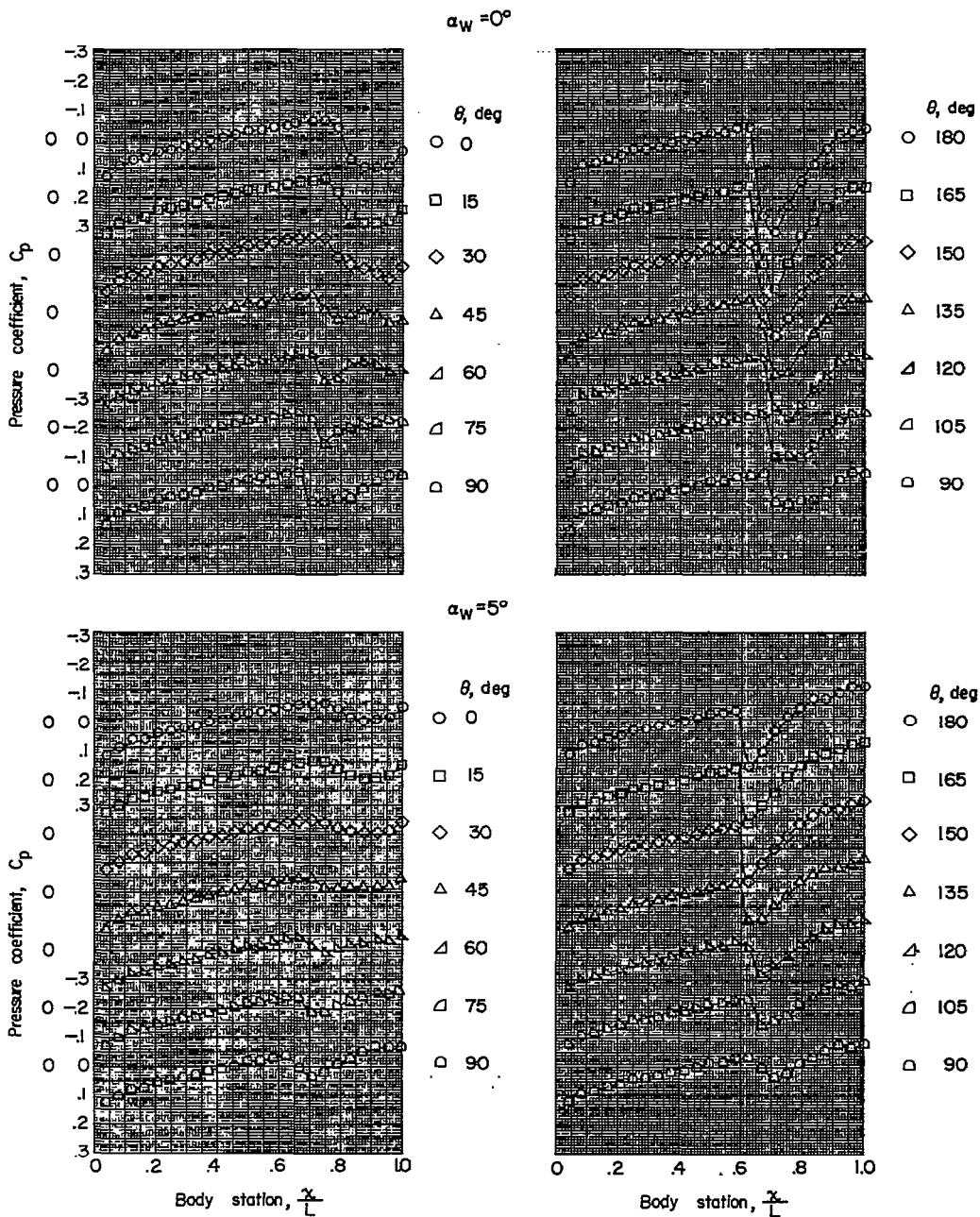
(e)  $X = -4$ ;  $Z = 1.5$ .

Figure 2.- Continued.



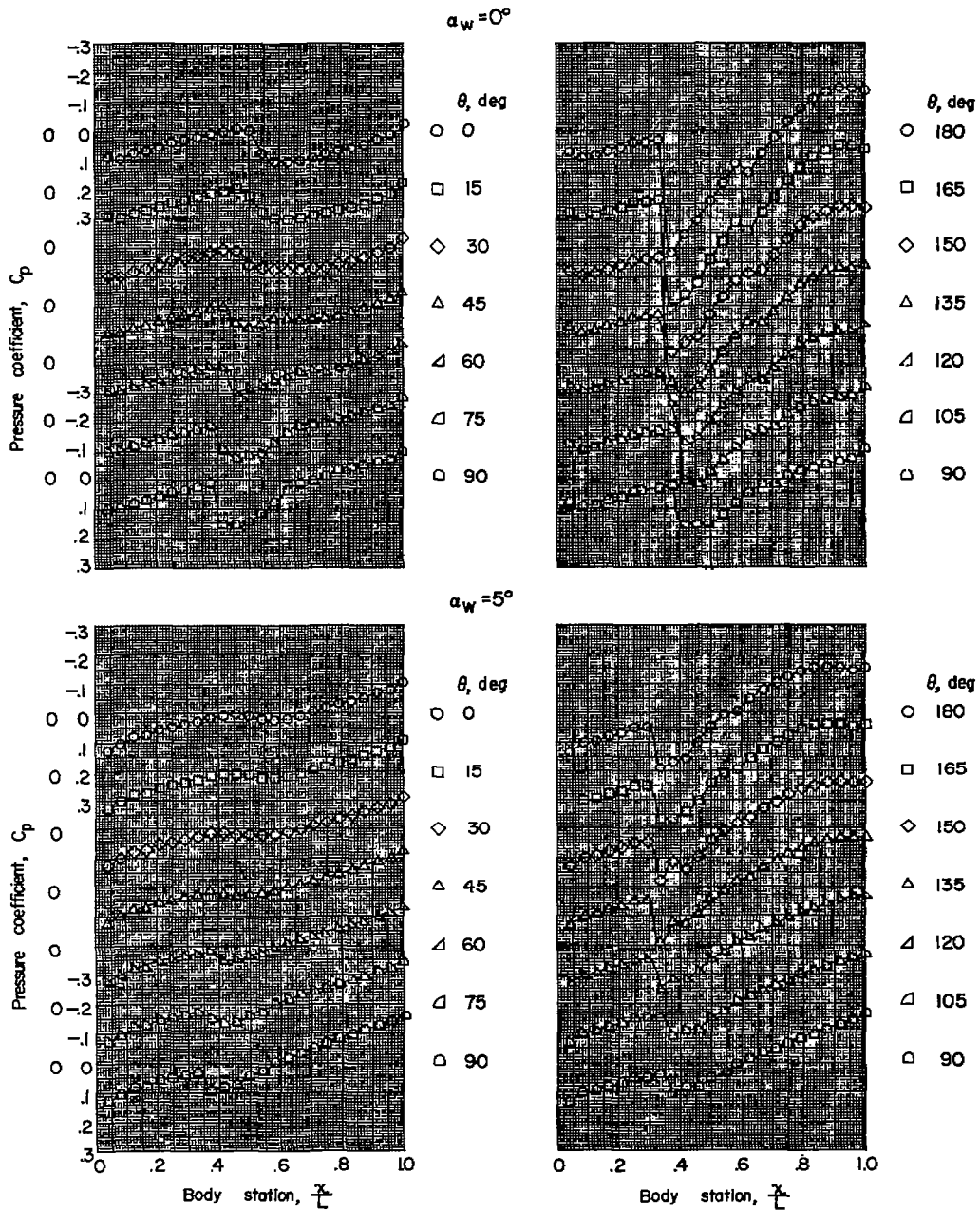
(f)  $X = -8; Z = 1.5$ .

Figure 2.- Continued.



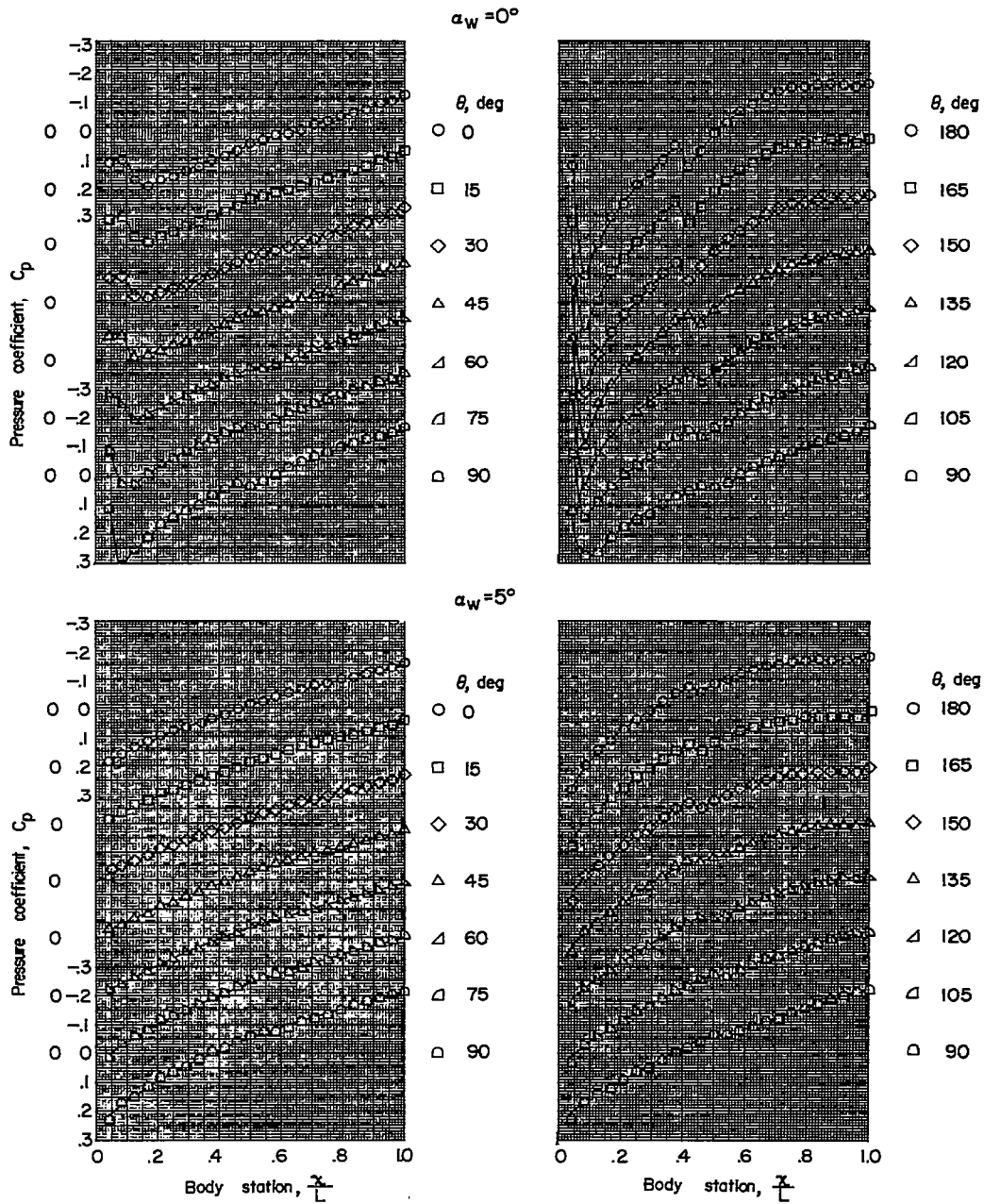
(g)  $X = 12; Z = 2.5.$

Figure 2.- Continued.



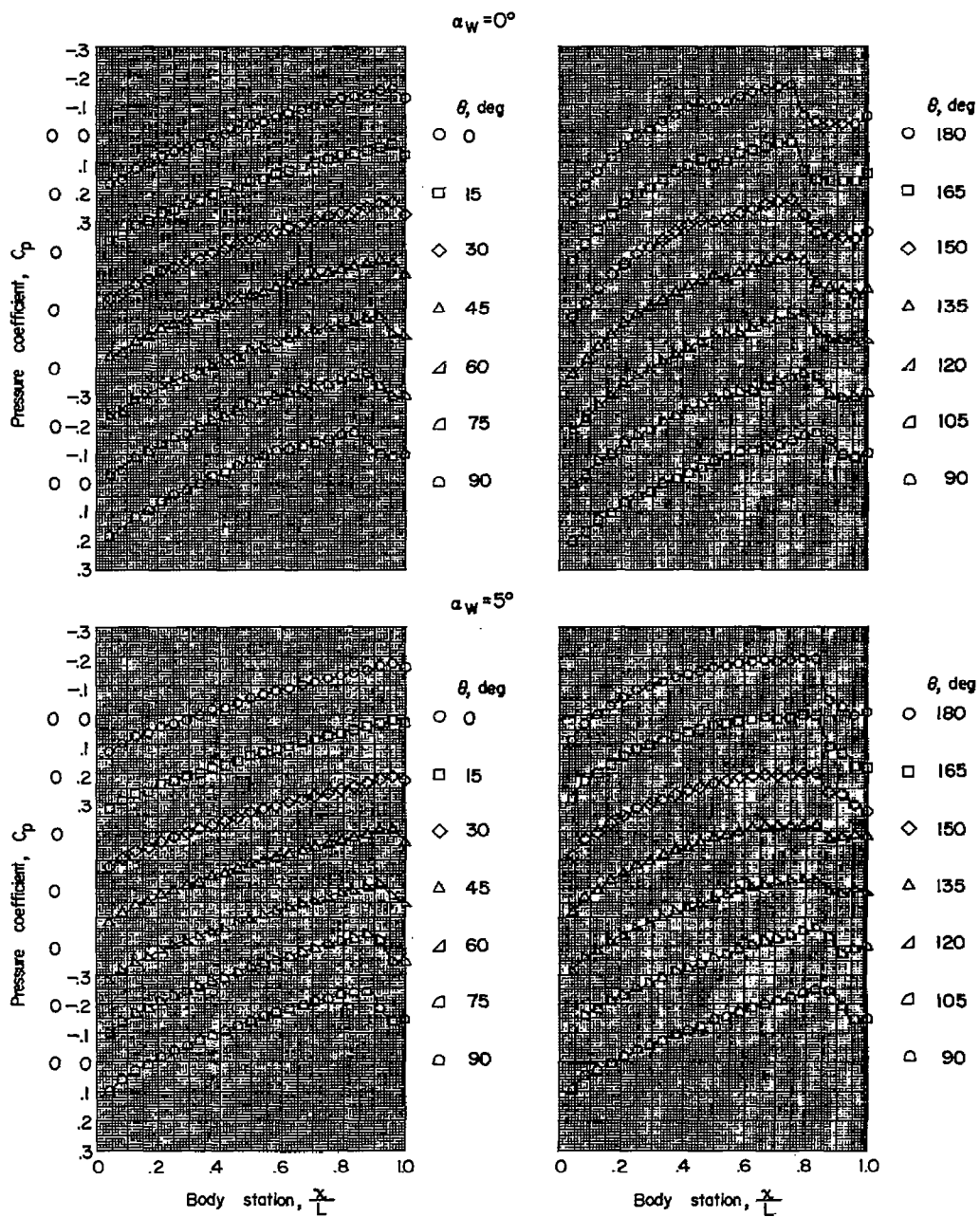
(h)  $X = 8; Z = 2.5.$

Figure 2.- Continued.



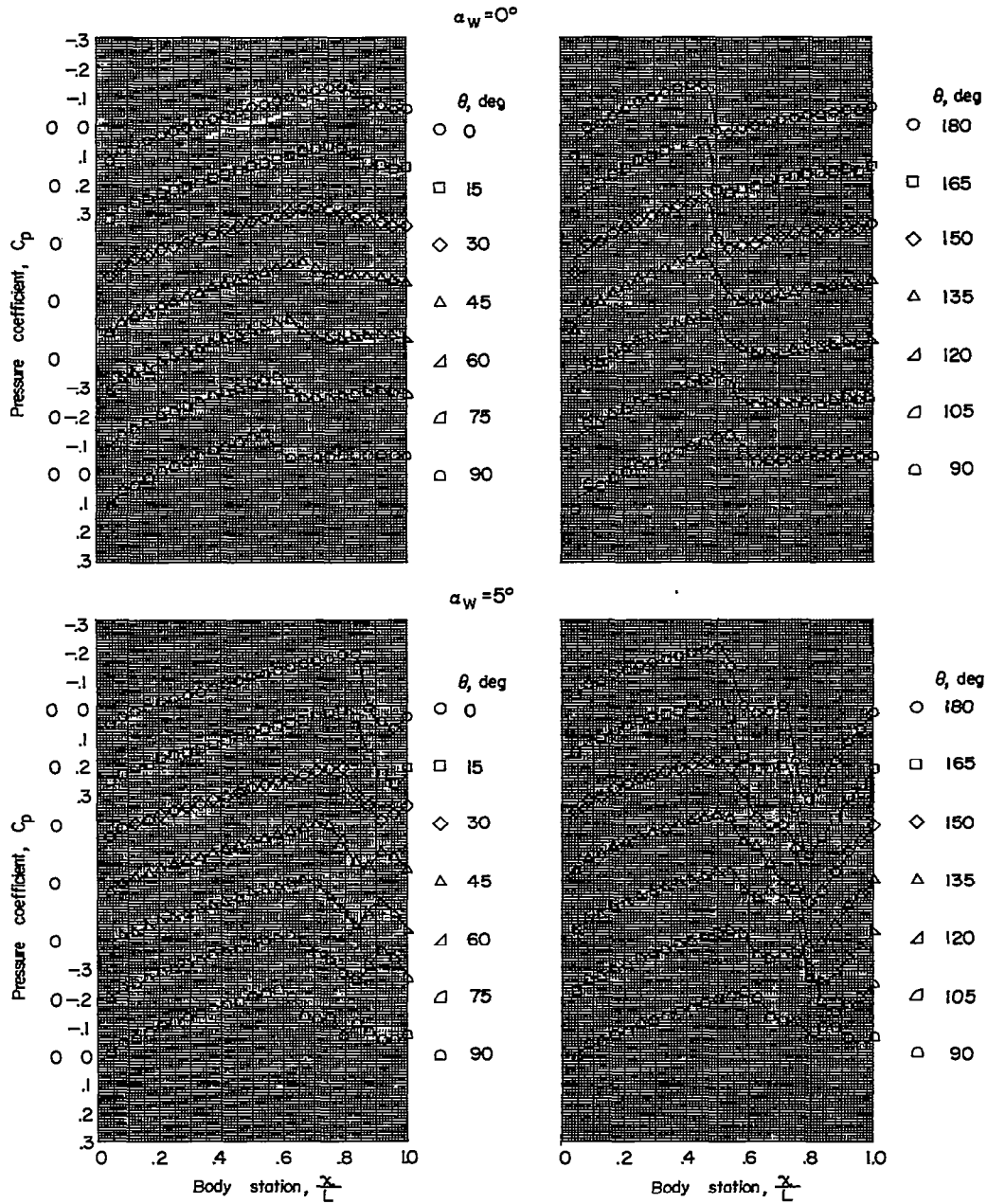
(1)  $X = 4; Z = 2.5.$

Figure 2.- Continued.



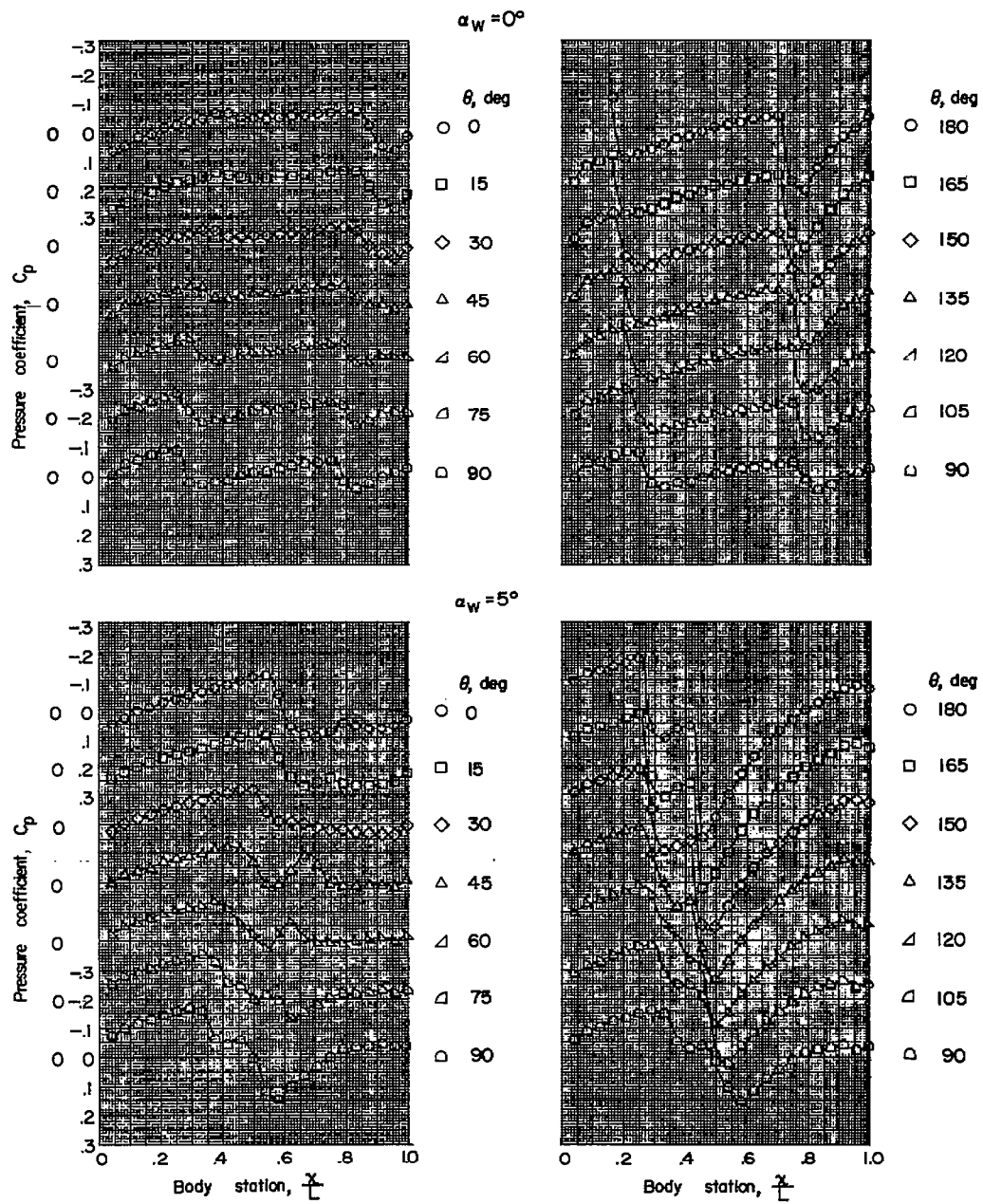
(j)  $X = 0; Z = 2.5.$

Figure 2.- Continued.



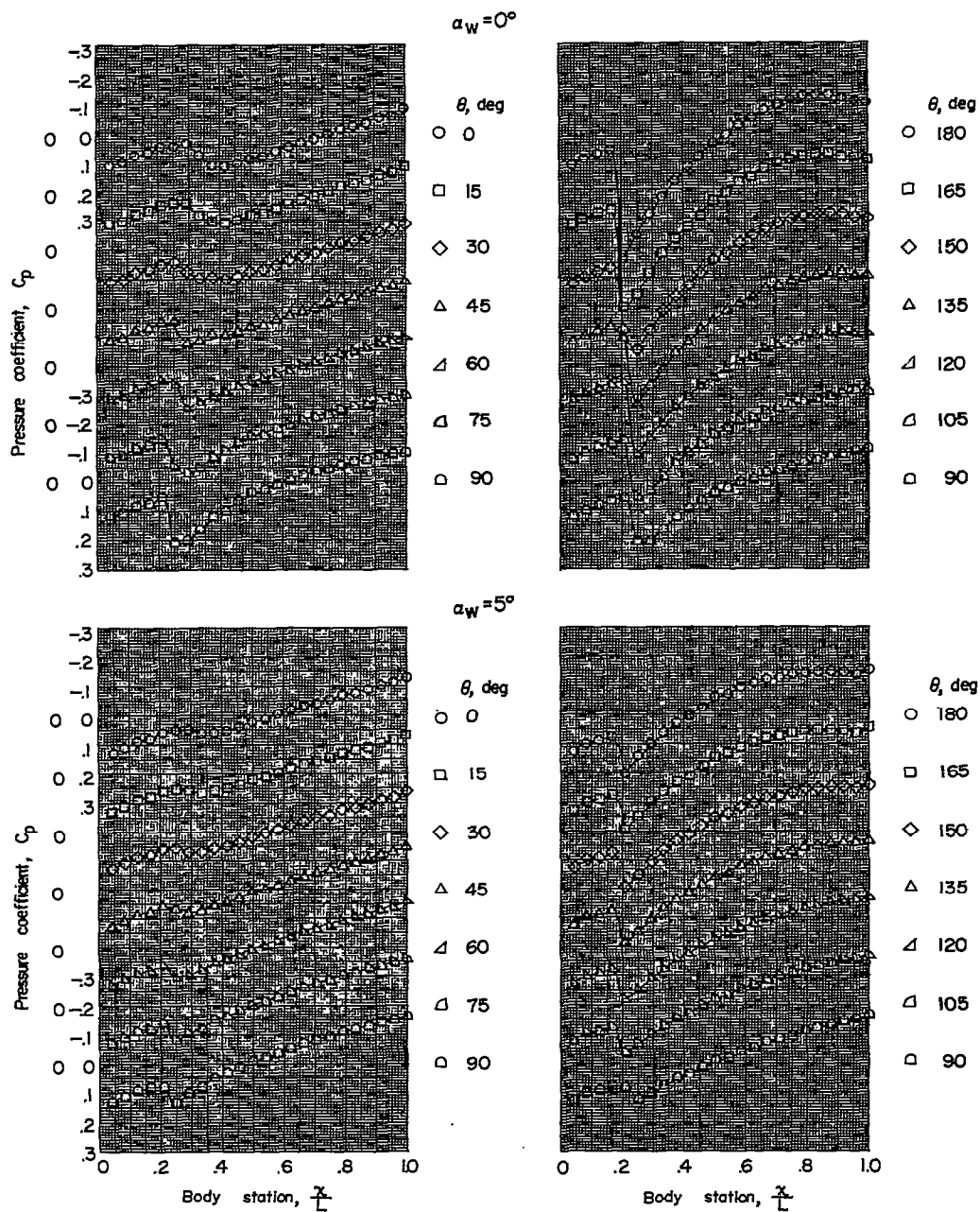
(k)  $X = -4; Z = 2.5.$

Figure 2.- Continued.



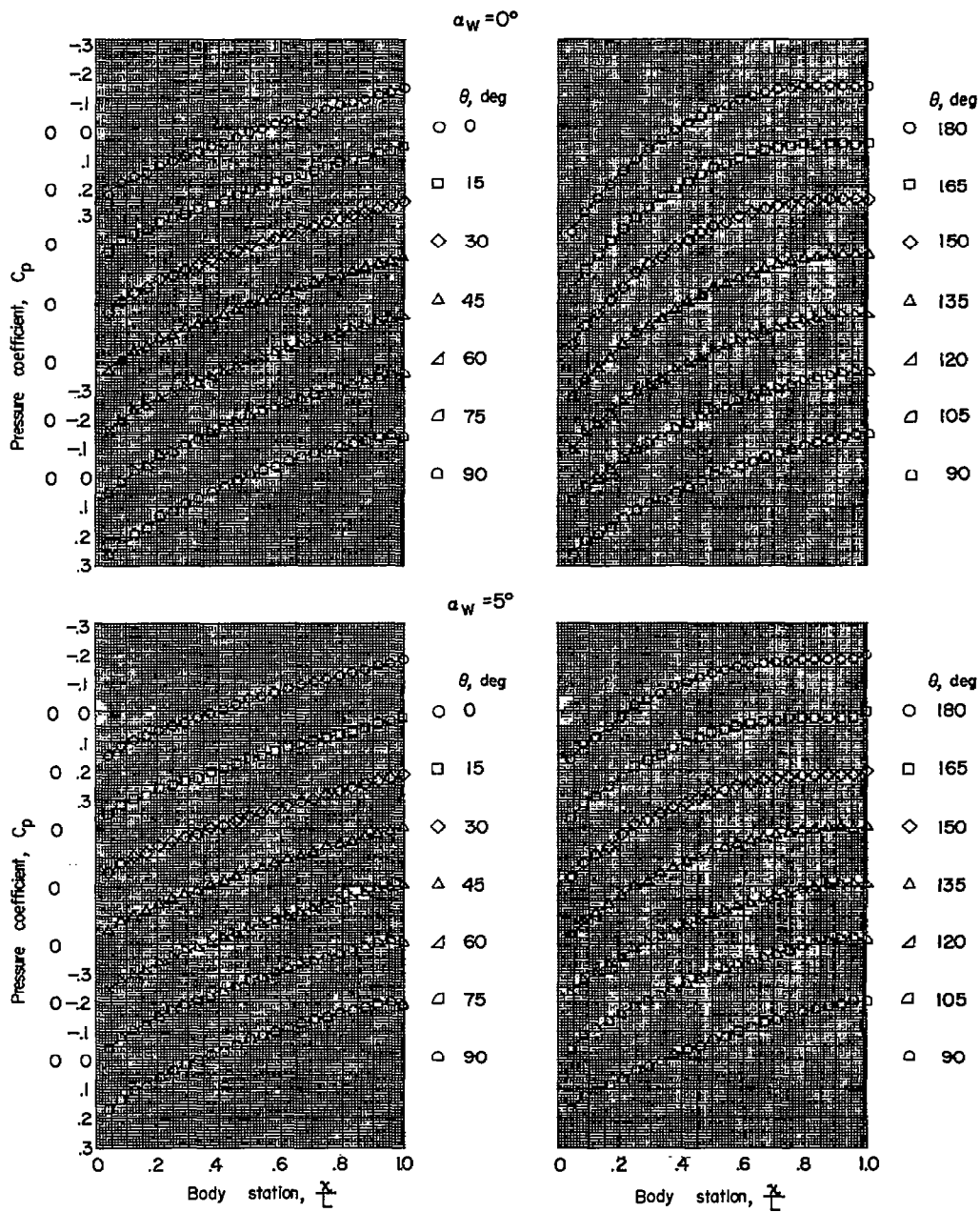
(1)  $X = -8; Z = 2.5$ .

Figure 2.- Continued.



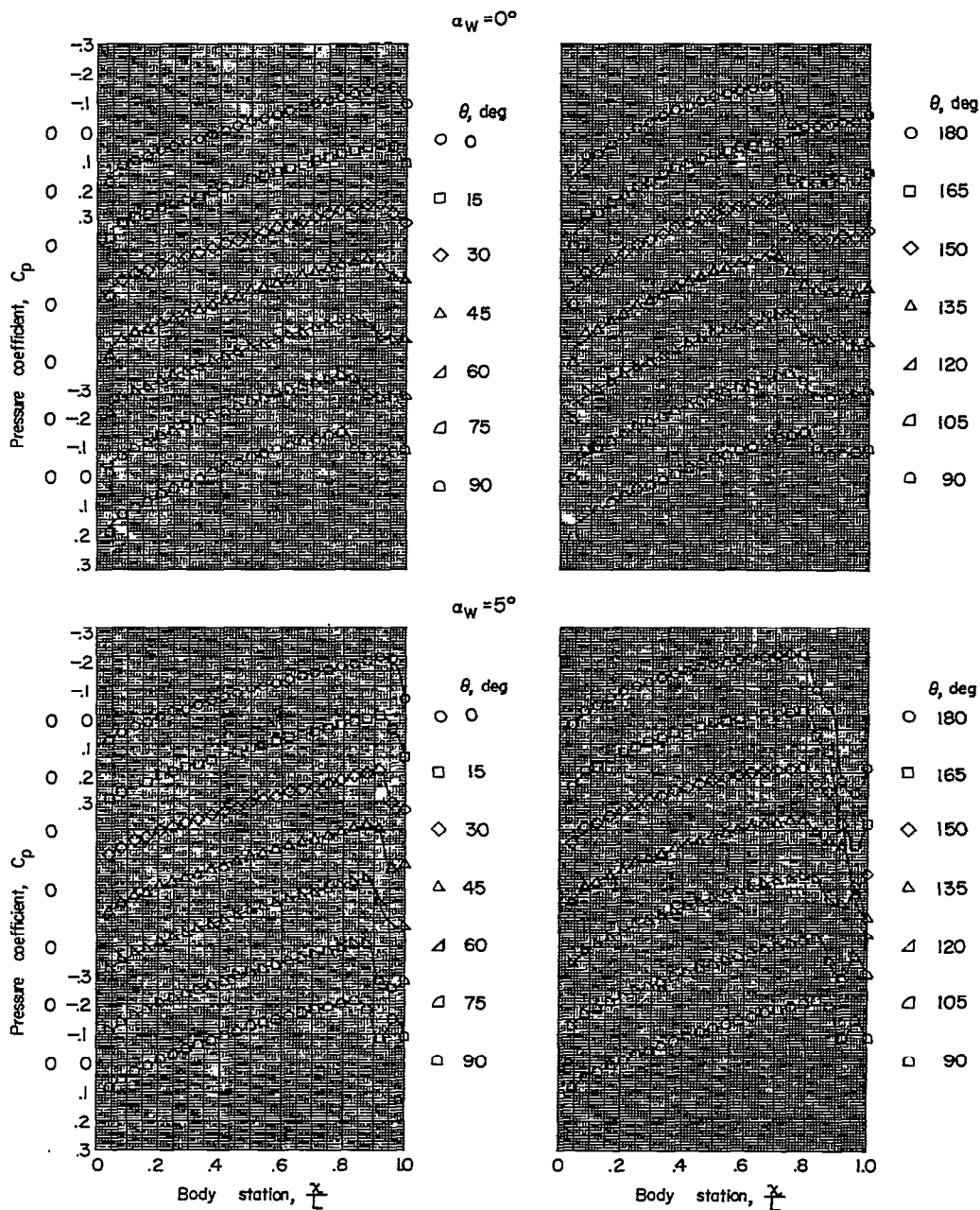
(m)  $X = 4; Z = 4.0.$

Figure 2.- Continued.



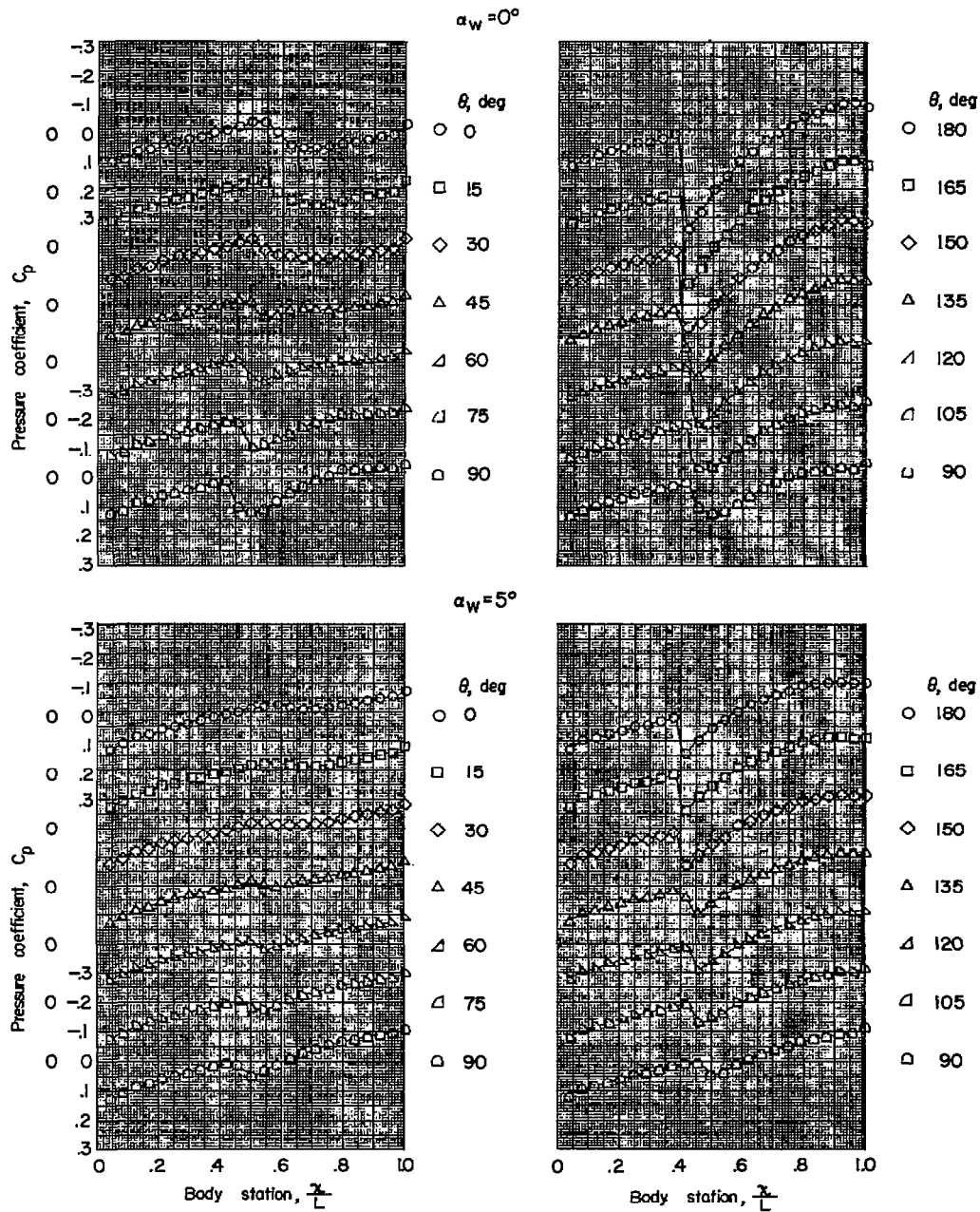
(n)  $X = 0$ ;  $Z = 4.0$ .

Figure 2.- Continued.



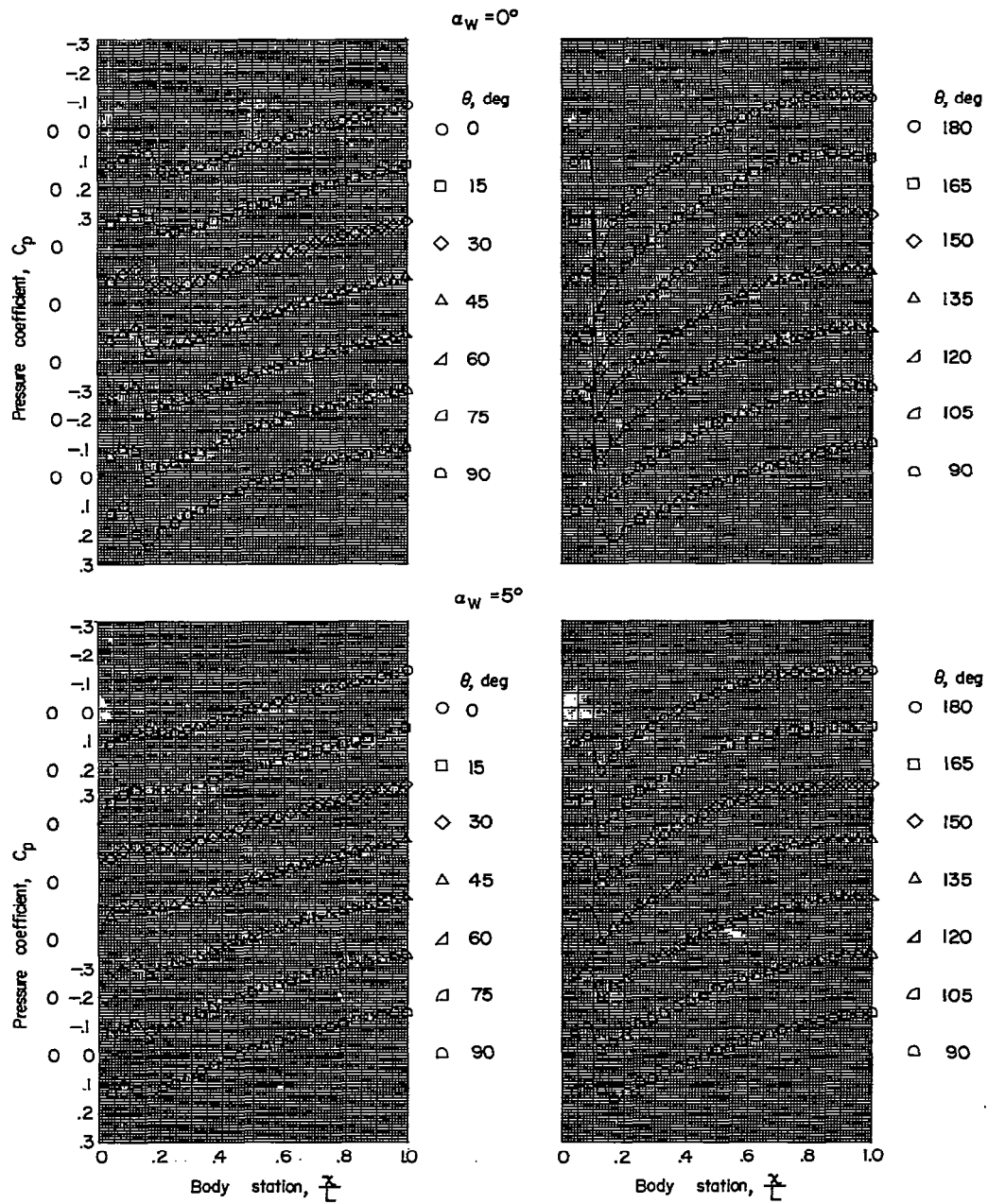
(o)  $X = -4; Z = 4.0.$

Figure 2.- Continued.



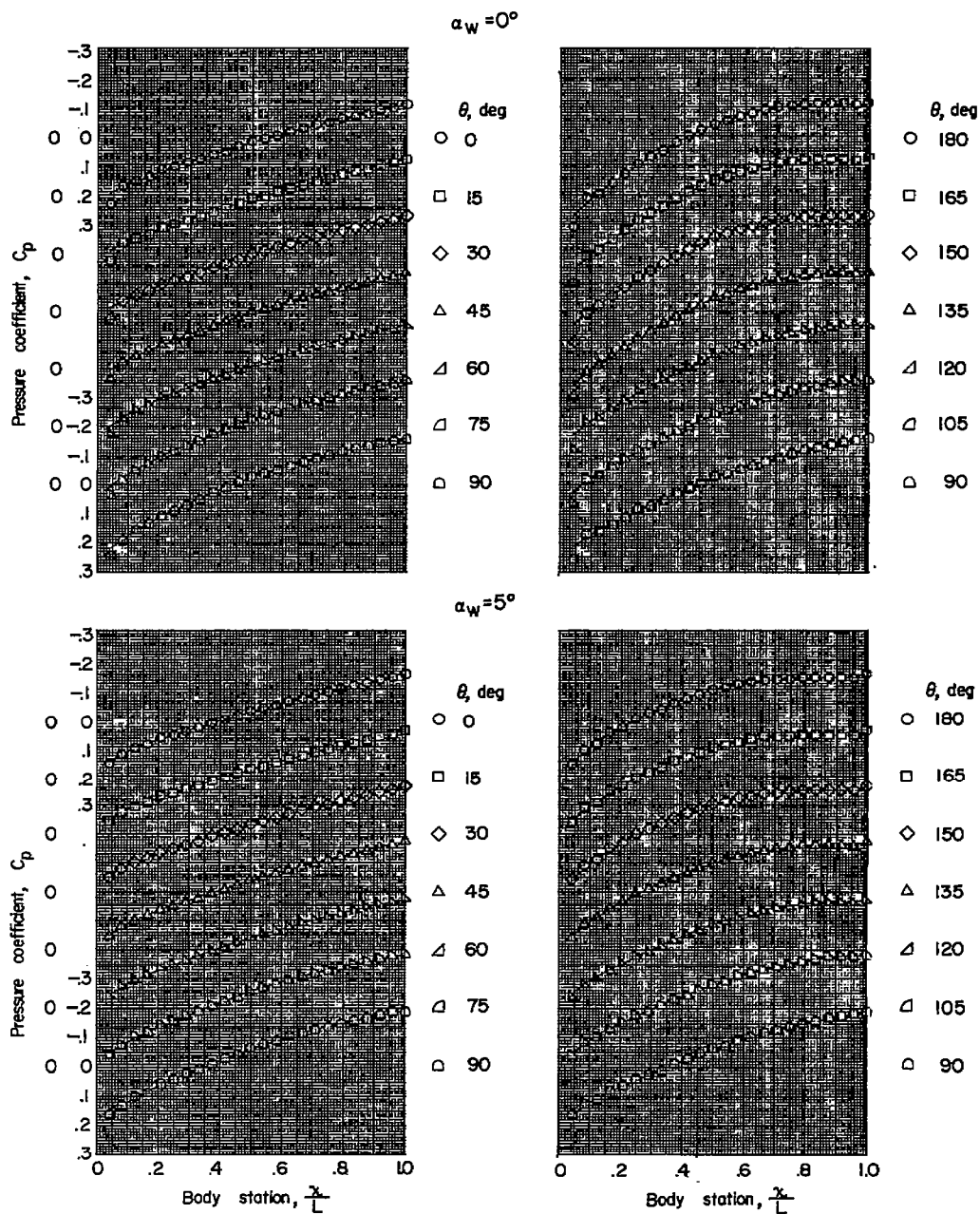
(p)  $X = 4; Z = 6.0.$

Figure 2.- Continued.



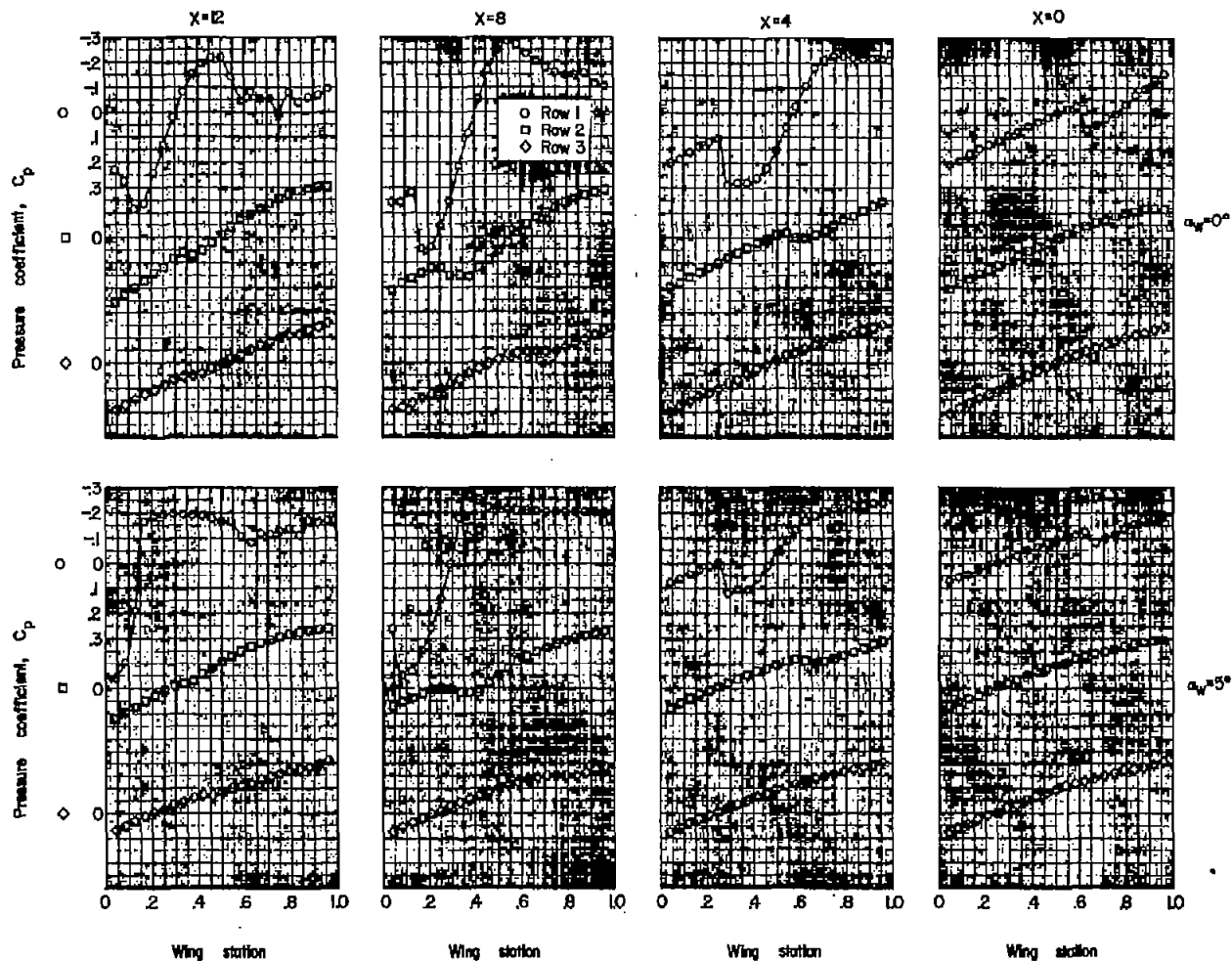
(q)  $X = 0; Z = 6.0.$

Figure 2.- Continued.



(r)  $X = -4; Z = 6.0.$

Figure 2.- Concluded.



(a)  $Z = 1.5$ .

Figure 3.- Pressure-coefficient variation on the wing for the various wing-body positions investigated.

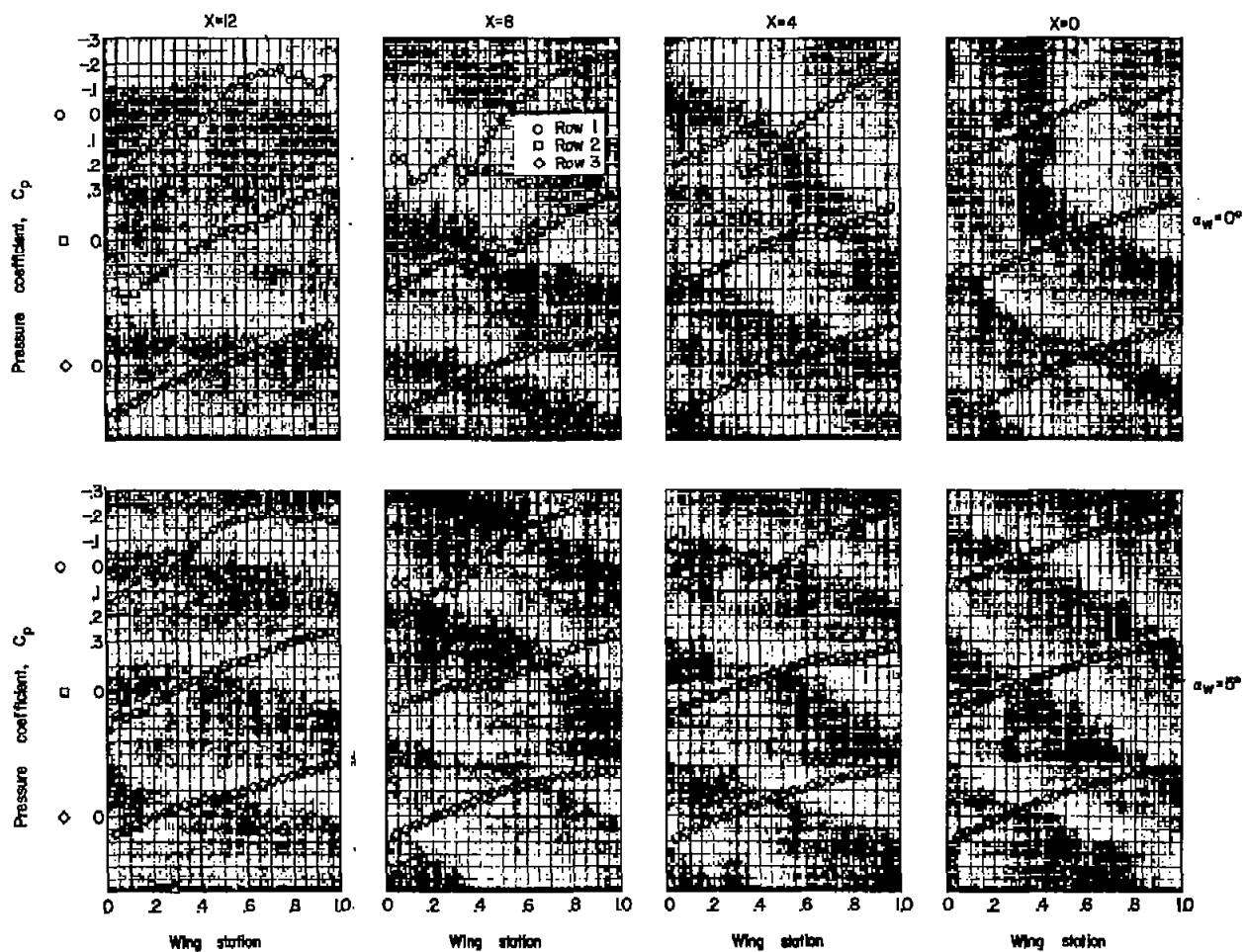
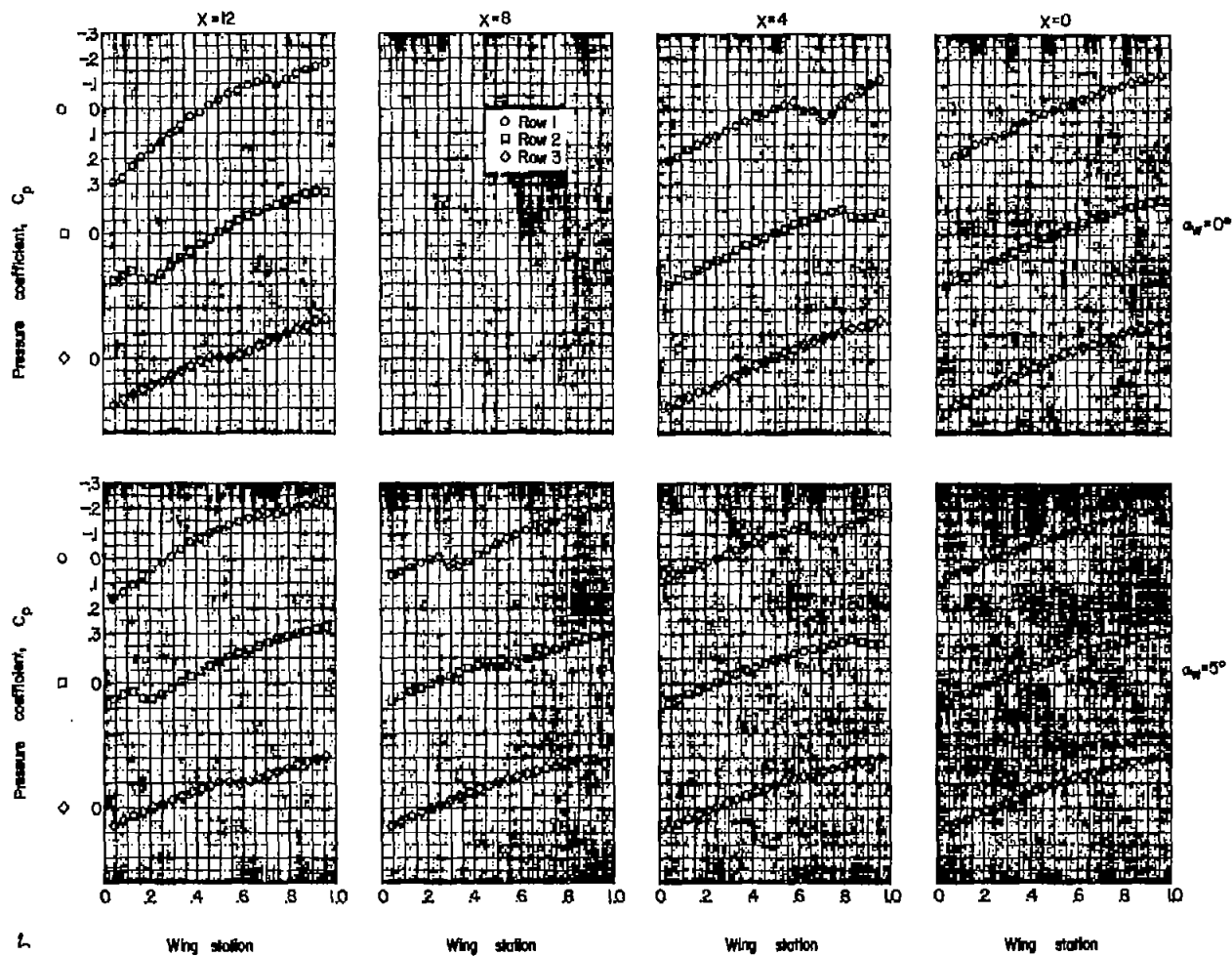
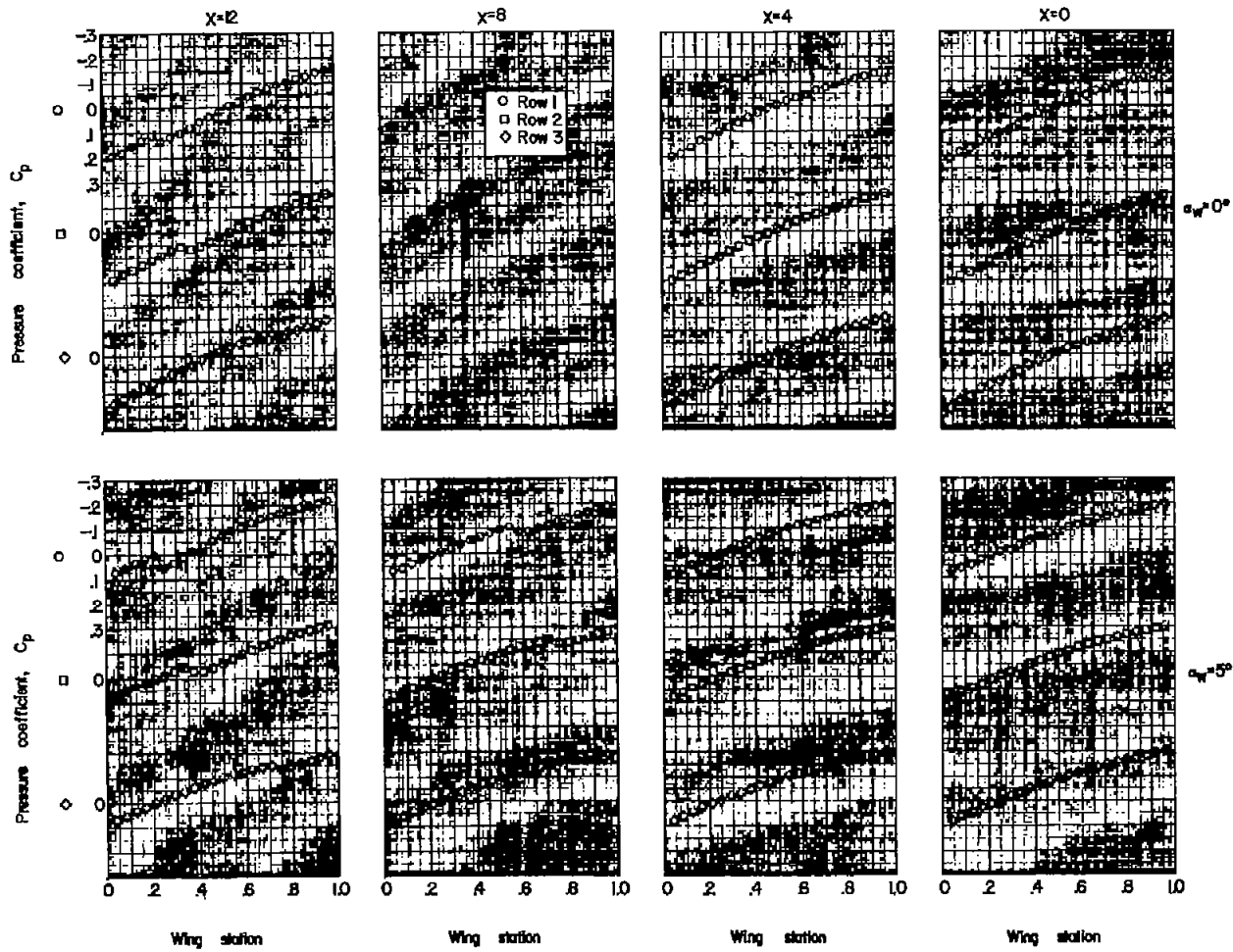


Figure 3.- Continued.



(c)  $Z = 4.0$ .

Figure 3.- Continued.



(d)  $z = 6.0$ .

Figure 3.- Concluded.

CONFIDENTIAL

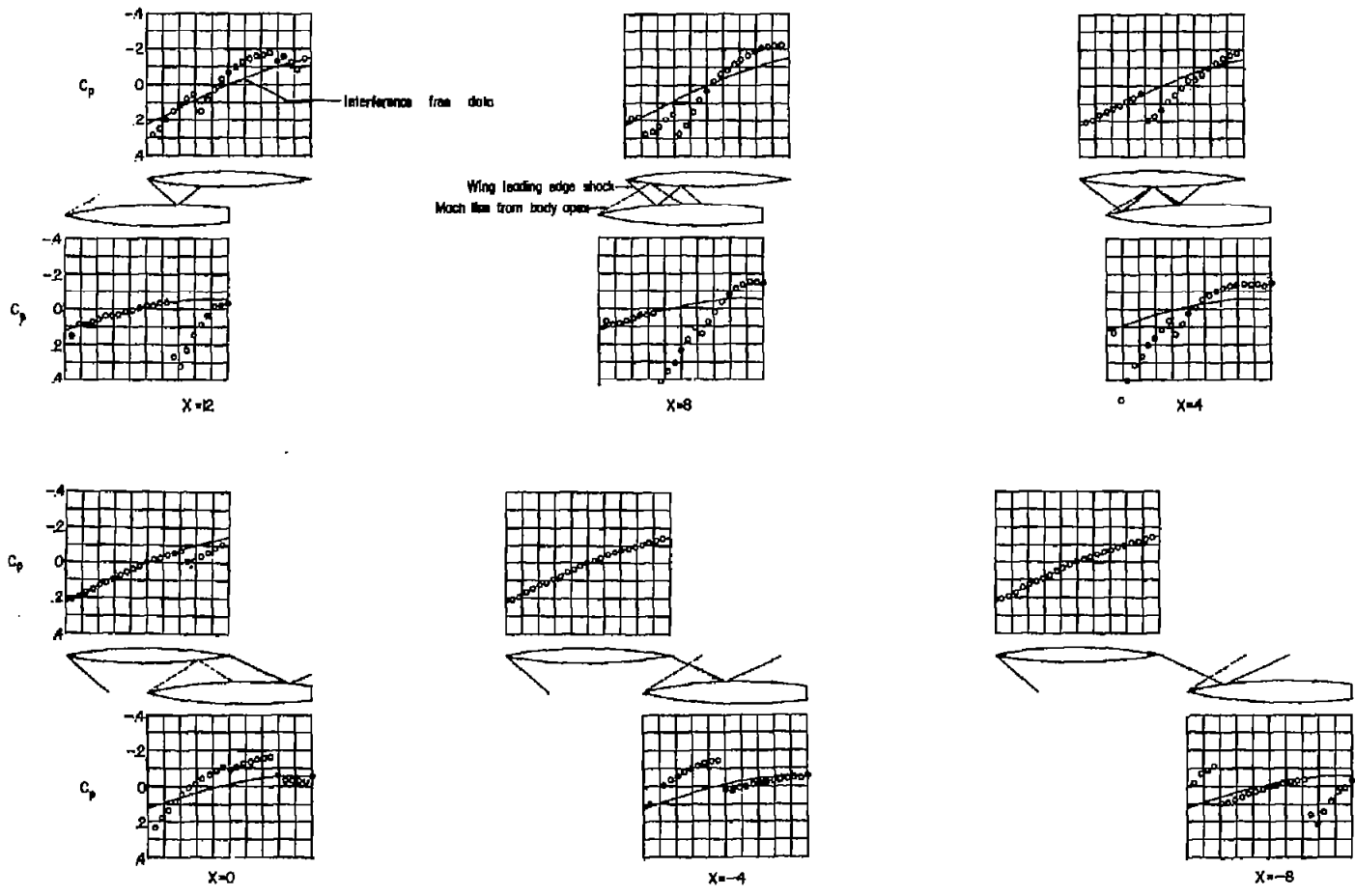


Figure 4.- Illustrative example of the pressure-coefficient variation on the body and wing as the body is moved through the wing flow field.  $Z = 2.5$ .

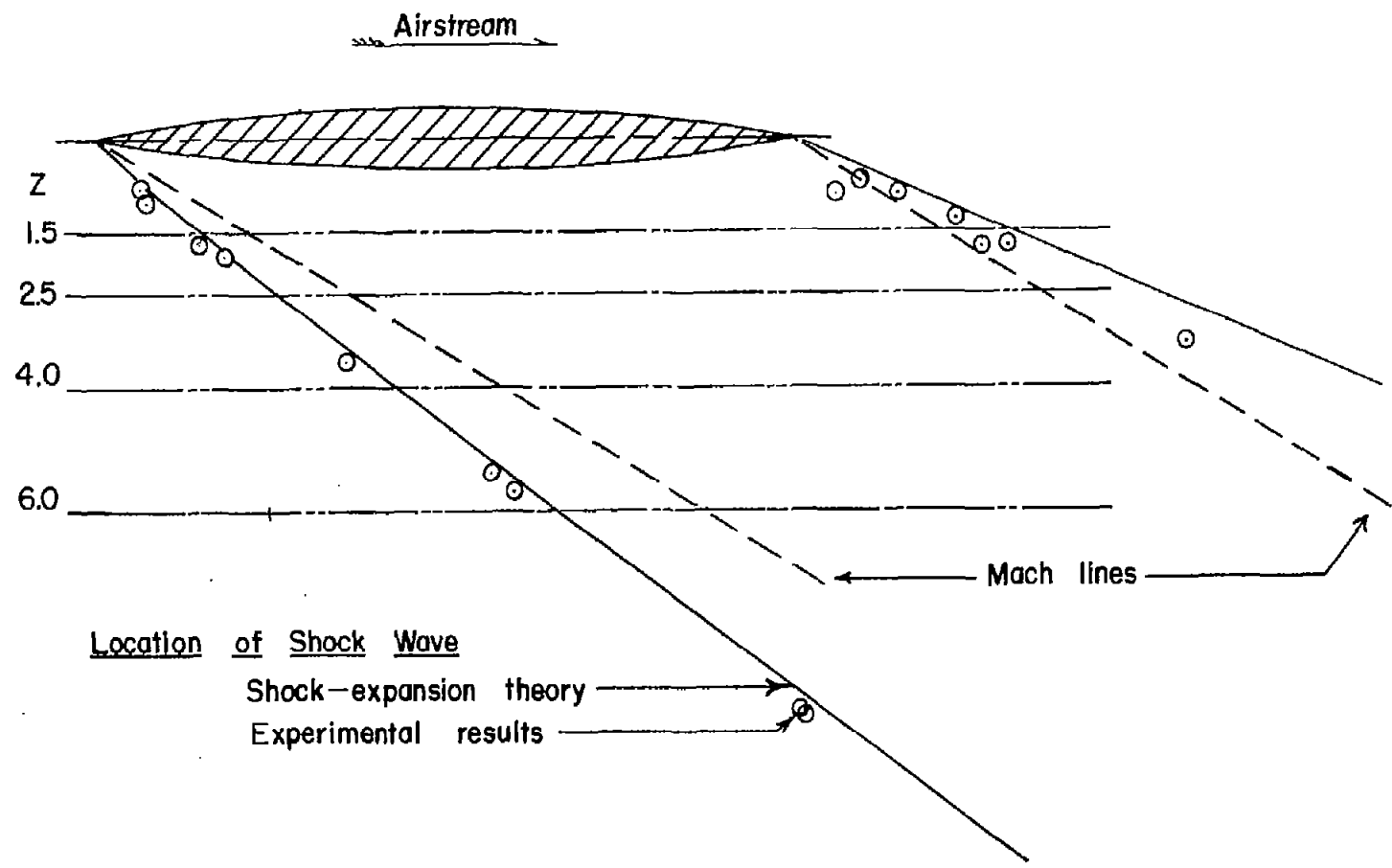


Figure 5.- Flow-field boundaries of an  $8\frac{1}{3}$ -percent-thick circular-arc wing.

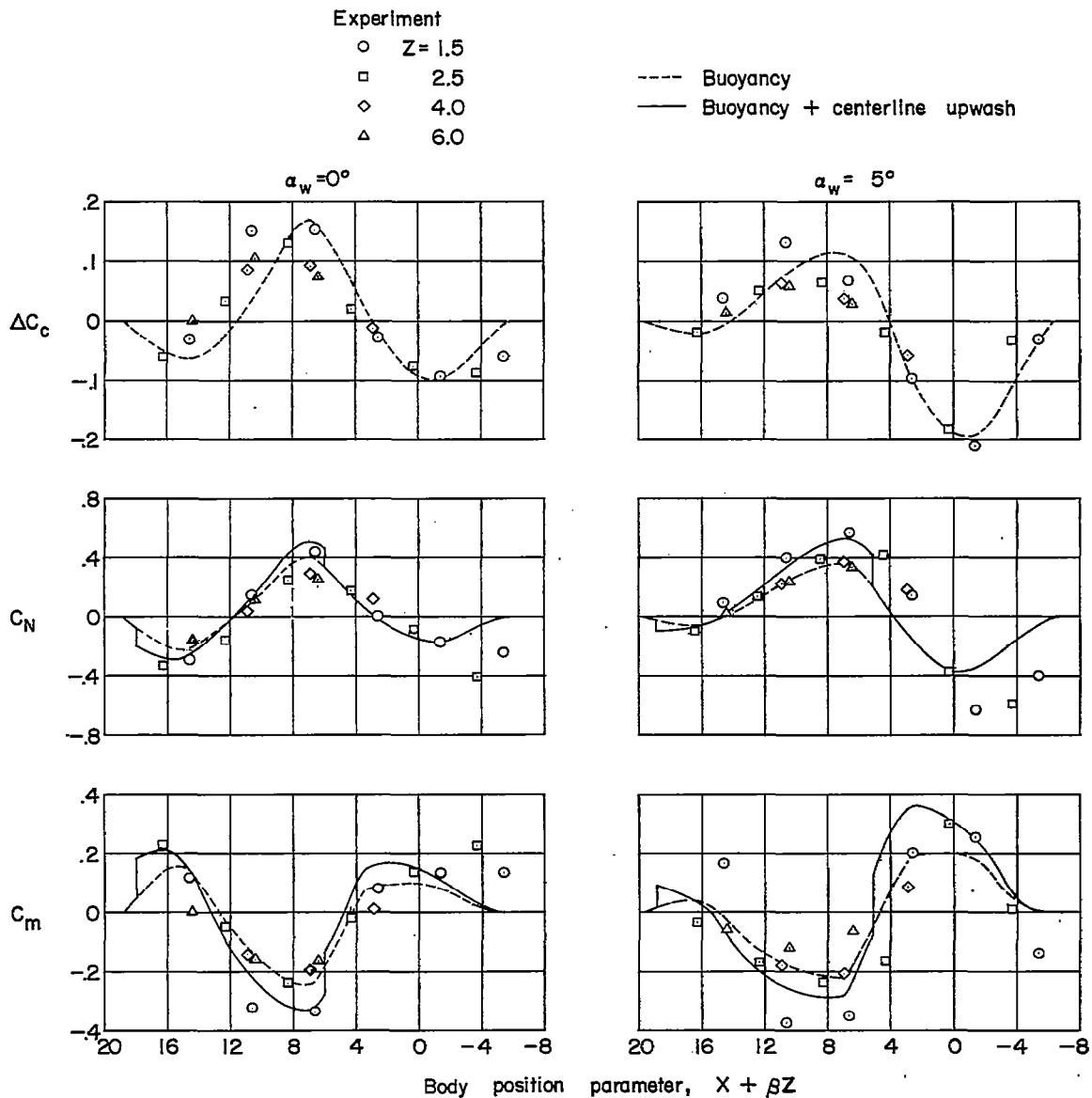


Figure 6.- Variation of the aerodynamic characteristics of the body as the body is moved through the wing flow field. Linearized wing-flow-field results.

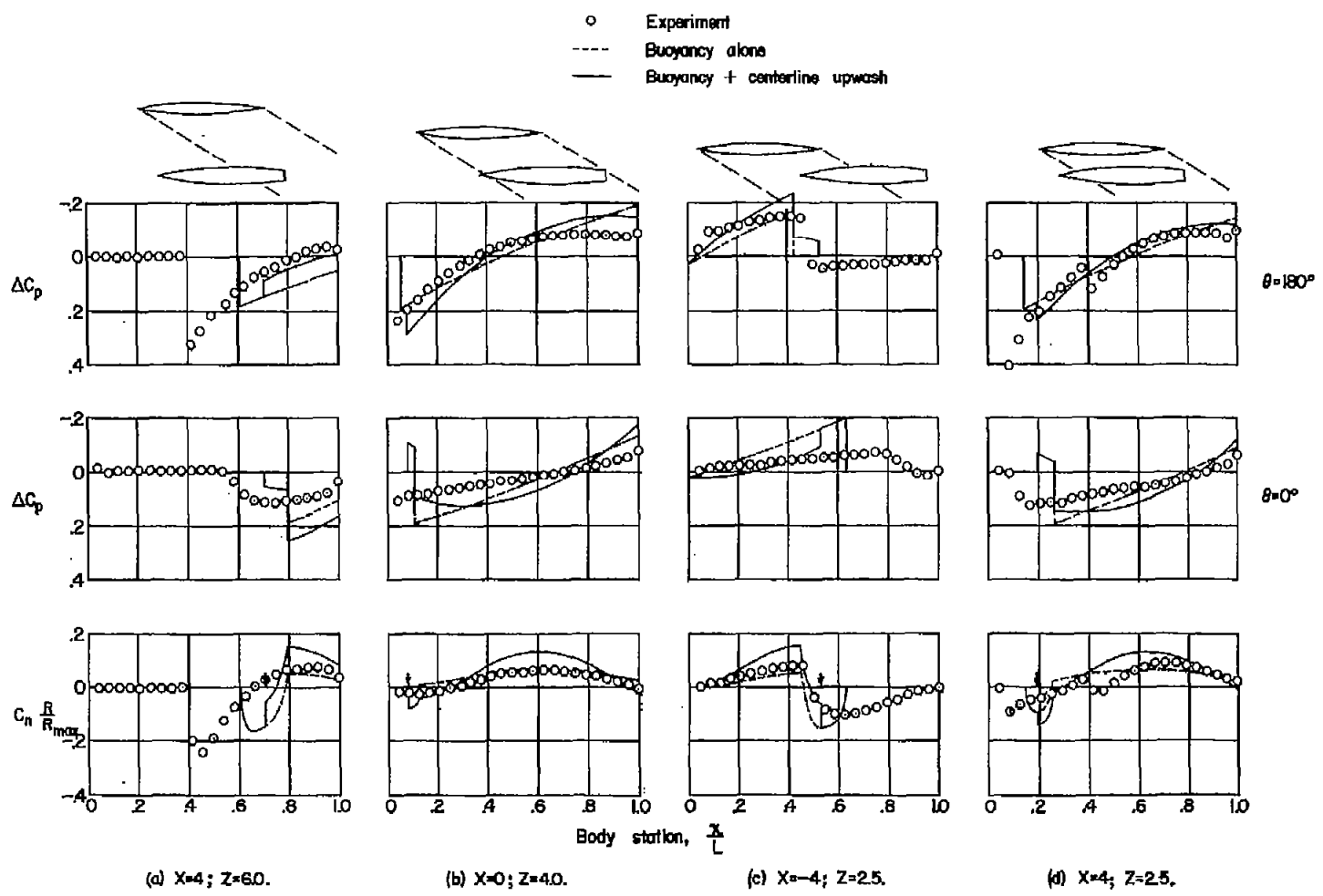


Figure 7.- Comparison between experimental and theoretical lifting pressure and normal-force loading distributions on the body for representative wing and body positions. Linearized wing-flow-field results. (Arrows indicate the position of the impulsive forces.)

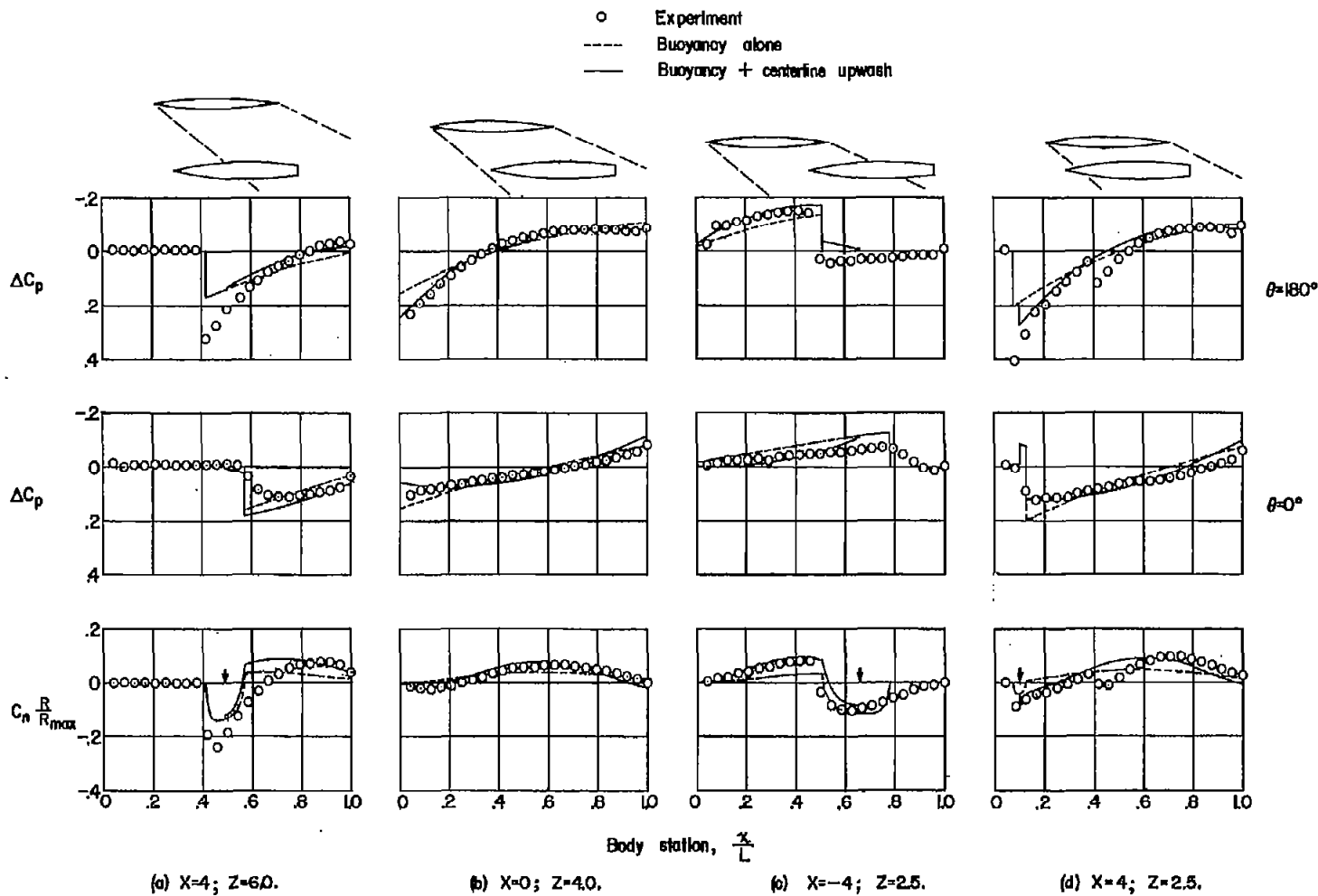
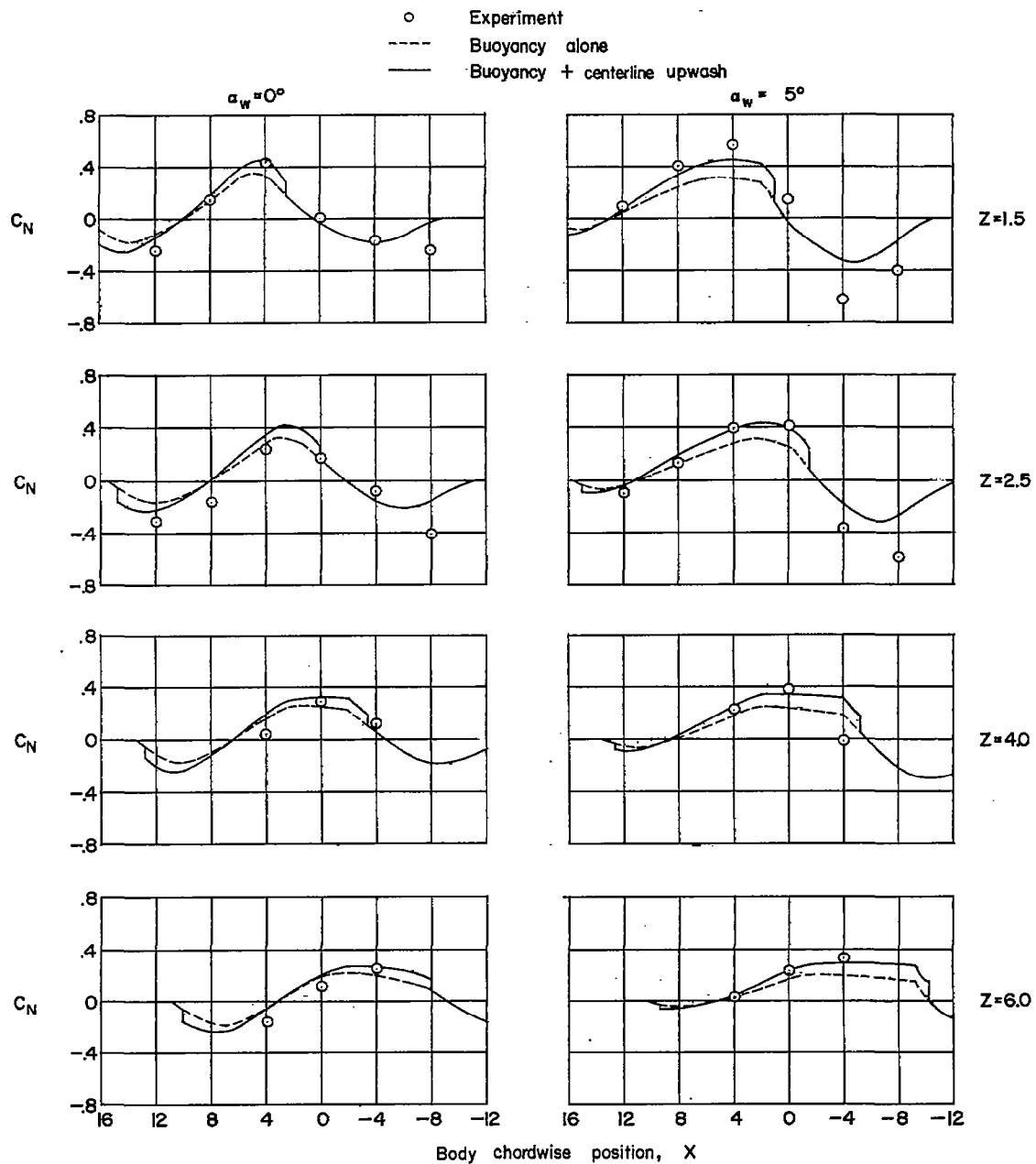


Figure 8.- Comparison between experimental and theoretical lifting pressure and normal-force loading distributions on the body for representative wing and body positions. Shock expansion wing-flow-field results. (Arrows indicate the position of the impulsive forces.)

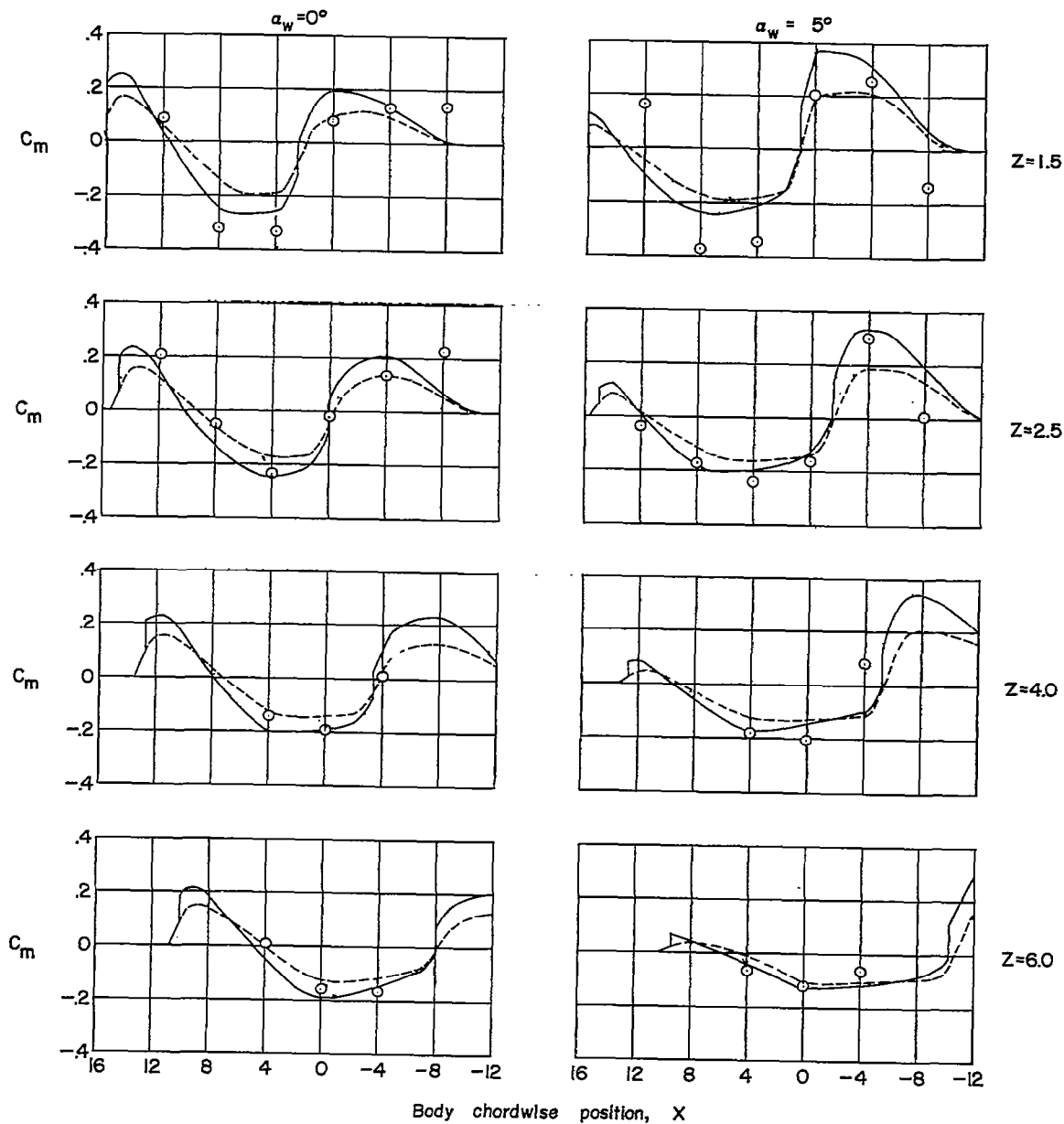


(a) Normal-force coefficient.

Figure 9.- Variation of the aerodynamic characteristics of the body as the body is moved through the wing flow field. Shock-expansion wing-flow-field results.

~~CONFIDENTIAL~~

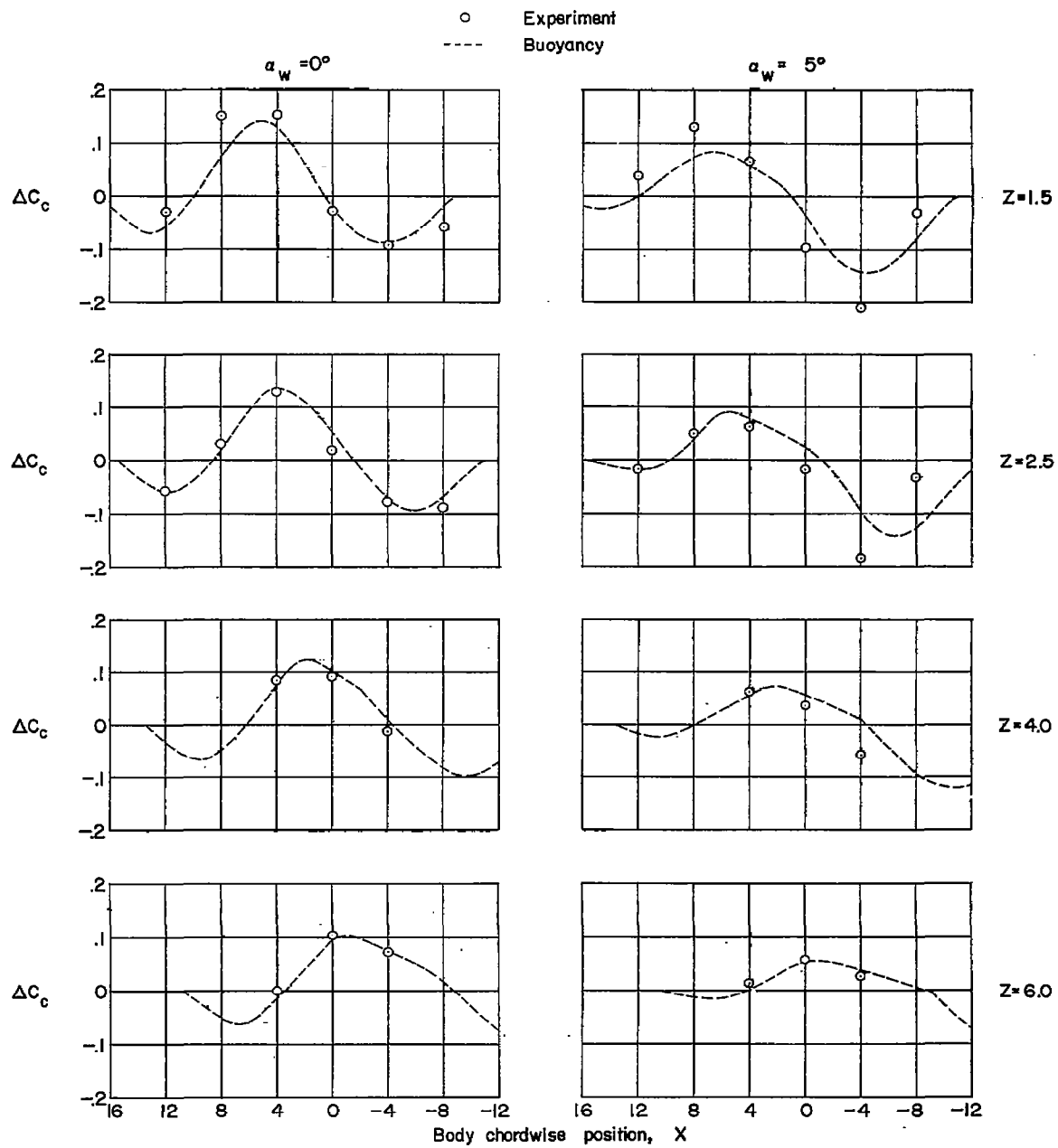
○ Experiment  
 - - - Buoyancy alone  
 — Buoyancy + centerline upwash



(b) Pitching-moment coefficient.

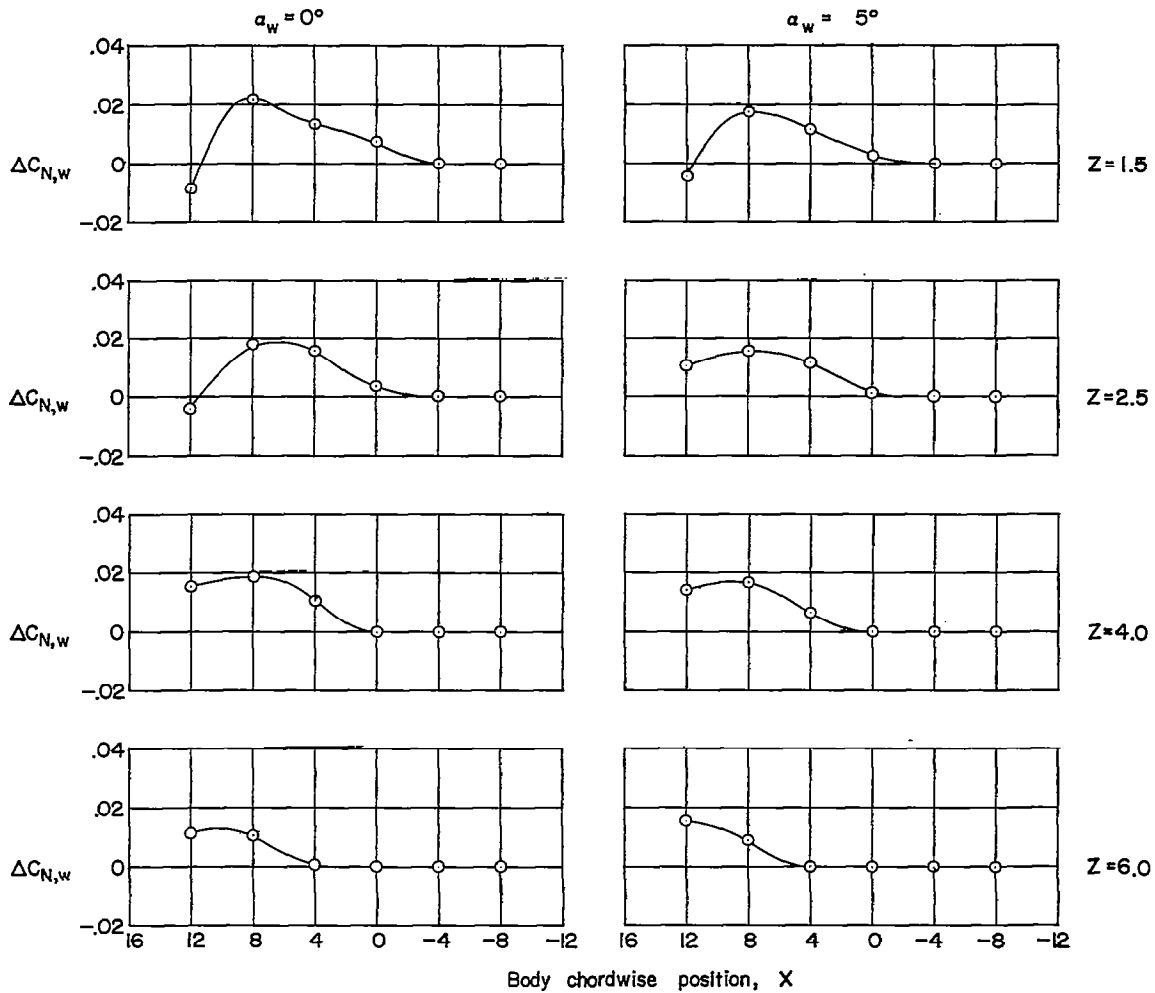
Figure 9.- Continued.

~~CONFIDENTIAL~~



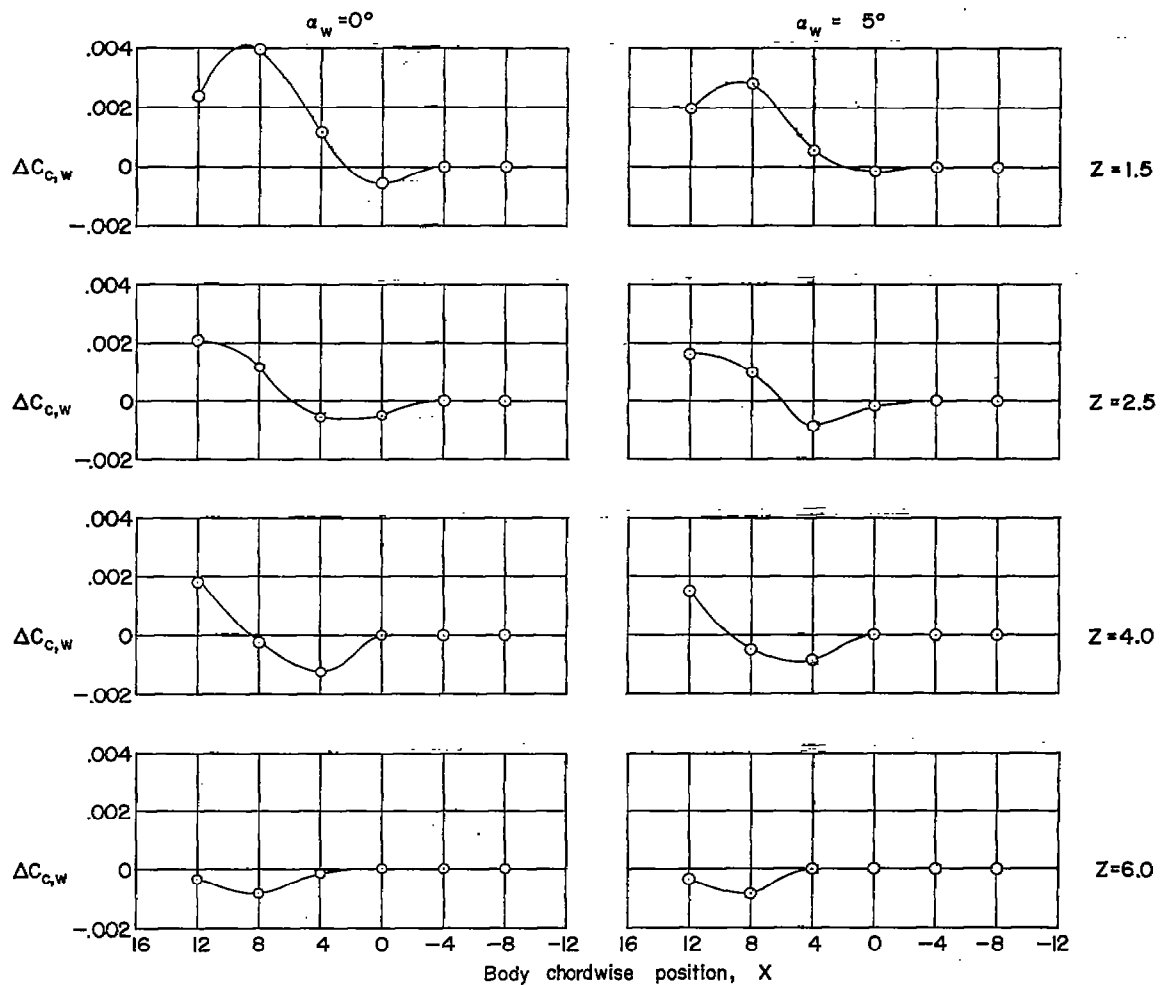
(c) Chord-force coefficient.

Figure 9.- Concluded.



(a) Normal-force coefficient.

Figure 10.- Variation of the aerodynamics characteristics of the wing as the body is moved through the wing flow field.



(b) Chord-force coefficient.

Figure 10.- Concluded.

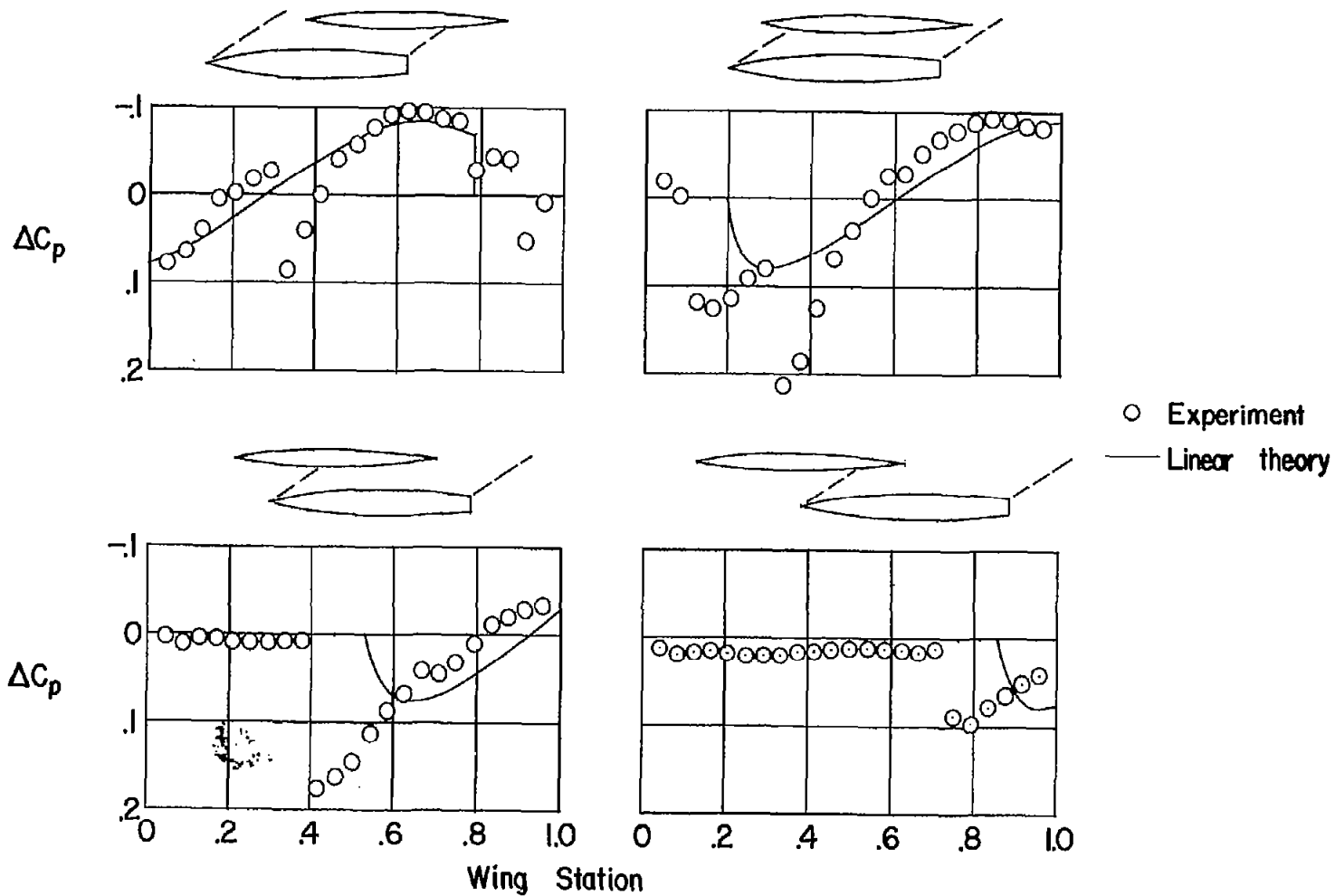


Figure 11.- Comparison between experimental and theoretical pressure distribution on the wing for representative wing and body locations.